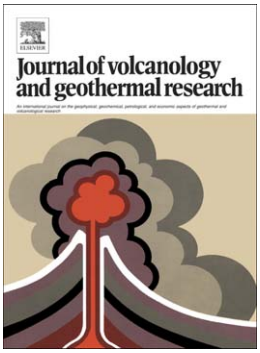

The latest explosive eruptions of Ciomadul (Csomád) volcano, East Carpathians — A tephrostratigraphic approach for the 51–29 ka BP time interval

D. Karátson, S. Wulf, D. Veres, E.K. Magyari, R. Gertisser, A. Timar-Gabor, Á. Novothny, T. Telbisz, Z. Szalai, V. Anechitei-Deacu, O. Appelt, M. Bormann, Cs. Jánosi, K. Hubay, F. Schäbitz

PII: S0377-0273(16)30014-2
DOI: doi: 10.1016/j.jvolgeores.2016.03.005
Reference: VOLGEO 5785

To appear in: *Journal of Volcanology and Geothermal Research*

Received date: 11 October 2015
Revised date: 4 March 2016
Accepted date: 6 March 2016

Please cite this article as: Karátson, D., Wulf, S., Veres, D., Magyari, E.K., Gertisser, R., Timar-Gabor, A., Novothny, Á., Telbisz, T., Szalai, Z., Anechitei-Deacu, V., Appelt, O., Bormann, M., Jánosi, Cs., Hubay, K., Schäbitz, F., The latest explosive eruptions of Ciomadul (Csomád) volcano, East Carpathians — A tephrostratigraphic approach for the 51–29 ka BP time interval, *Journal of Volcanology and Geothermal Research* (2016), doi: 10.1016/j.jvolgeores.2016.03.005

The latest explosive eruptions of Ciomadul (Csomád) volcano, East Carpathians - a tephrostratigraphic approach for the 51–29 ka BP time interval

Karátson, D.[1], Wulf, S.[2, 3], Veres, D.[4] , Magyari, E.K.[5], Gertisser, R.[6], Timar-Gabor, A.[7, 8], Novothny, Á.[1], Telbisz, T.[1], Szalai, Z.[9, 10] Anechitei-Deacu, V.[7,8], Appelt, O.[11], Bormann, M.[12], Jánosi, Cs.[13], Hubay, K. [14], Schäbitz, F.[12]

[1]Eötvös University, Department of Physical Geography, Pázmány s. 1/C, H-1117 Budapest, HUNGARY
[2]GFZ German Research Centre for Geosciences, Section 5.2 - Climate Dynamics and Landscape Evolution, Telegrafenberg, D-14473 Potsdam, GERMANY
[3]Senckenberg Research Institute and Natural History Museum, BIK-F, TSP6 Evolution and Climate, Senckenberganlage 25, D-60325 Frankfurt a.M., GERMANY
[4]Institute of Speleology, Romanian Academy, Clinicilor 5, 400006 Cluj-Napoca, ROMANIA
[5]Eötvös University, MTA-MTM-ELTE Research Group for Paleontology, Pázmány s. 1/C, H-1117 Budapest, HUNGARY
[6]Keele University, School of Physical and Geographical Sciences, Keele, ST5 5BG, UK
[7]Interdisciplinary Research Institute on Bio-Nano-Science, Babeş-Bolyai University, Treboniu Laurean str. 42, RO-400271 Cluj-Napoca, ROMANIA
[8]Faculty of Environmental Sciences and Engineering, Babeş-Bolyai University, Fantanele str. 30, RO-400294 Cluj-Napoca, ROMANIA
[9]Eötvös University, Department of Environmental and Landscape Geography, Pázmány s. 1/C, H-1117 Budapest, HUNGARY
[10]Research Centre for Astronomy and Earth Sciences, Hungarian Academy of Sciences, Budaörsi út 45, H-1112 Budapest, HUNGARY
[11]GFZ German Research Centre for Geosciences, Section 4.3, Chemistry and Physics of Earth Materials, Telegrafenberg, D-14473 Potsdam, GERMANY
[12]University of Cologne, Institute of Geography Education, Gronewaldstr 2, D-50931 Cologne, GERMANY
[13]Inimii 3/14, RO-530225 Miercurea Ciuc, ROMANIA
[14]Hertelendi Laboratory of Environmental Studies, Atomki, 4026 Debrecen, Bem tér 18/c, HUNGARY

Keywords:
Ciomadul; tephrostratigraphy; Quaternary; Carpathians; radiometric chronology

Abstract

The most recent, mainly explosive eruptions of Ciomadul, the youngest volcano in the Carpatho-Pannonian Region, have been constrained by detailed field volcanological studies, major element pumice glass geochemistry, luminescence and radiocarbon dating, and a critical evaluation of available geochronological data. These investigations were complemented by the first tephrostratigraphic studies of the lacustrine infill of Ciomadul's twin craters (St. Ana and Mohoş) that received tephra deposition during the last eruptions of the volcano. Our analysis shows that significant explosive activity, collectively called EPPA (Early Phreatomagmatic and Plinian Activity), started at Ciomadul in or around the present-

day Mohoş, the older crater, at ≥51 ka BP. These eruptions resulted in a thick succession of pyroclastic-fall deposits found in both proximal and medial/distal localities around the volcano, characterized by highly silicic (rhyolitic) glass chemical compositions (ca. 75.2-79.8 wt% SiO_2). The EPPA stage was terminated by a subplinian/plinian eruption at ≥43 ka BP, producing pumiceous pyroclastic-fall and -flow deposits of similar glass composition, probably from a "Proto-St. Ana" vent located at or around the younger crater hosting the present-day Lake St. Ana. After a quiescent period with a proposed lava dome growth in the St. Ana crater, a new explosive stage began, defined as MPA (Middle Plinian Activity). In particular, a significant two-phase eruption occurred at ~31.5 ka BP, producing pyroclastic flows from vulcanian explosions disrupting the preexisting lava dome of Sf. Ana, and followed by pumiceous fallout from a plinian eruption column. Related pyroclastic deposits show a characteristic, less evolved rhyolitic glass composition (ca. 70.2-74.5 wt% SiO_2) and occur both in proximal and medial/distal localities up to 21 km from source. The MPA eruptions, that may have pre-shaped a crater similar to, but possibly smaller than, the present-day St. Ana crater, was followed by a so far unknown, but likewise violent last eruptive stage from the same vent, creating the final morphology of the crater. This stage, referred to as LSPA (Latest St. Ana Phreatomagmatic Activity), produced pyroclastic-fall deposits of more evolved rhyolitic glass composition (ca. 72.8-78.8 wt% SiO_2) compared to that of the previous MPA stage. According to radiocarbon age constraints on bulk sediment, charcoal and organic matter from lacustrine sediments recovered from both craters, the last of these phreatomagmatic eruptions—that draped the landscape toward the east and southeast of the volcano—occurred at ~29.6 ka BP, some 2,000 years later than the previously suggested last eruption of Ciomadul.

1. Introduction

In the past decade, a significant number of papers has been published in the on the eruptive history of Ciomadul (Csomád)[1] volcano, East Carpathians, Romania (e.g., Karátson, 2007; Vinkler et al., 2007; Harangi et al., 2010, 2015; Popa et al., 2012; Karátson et al., 2013; Szakács et al., 2015), revitalizing the research on this Late Pleistocene twin-cratered explosive dacitic lava dome complex. Moreover, the volcanological approach has been associated with a growing interest in Quaternary science, recognizing its potential of regional palaeoclimate reconstruction using the lacustrine sedimentary infills of the two craters (Lake Sfânta Ana [Szent Anna], hereafter St. Ana) and Mohoș [Mohos] peat bog), that led to new age constraints of the final crater-forming events (e.g., Tanțau, 2003; Magyari et al., 2006, 2009, 2014; Panait and Tanțau, 2012). These works cast new light on the hazard and risk assessment of Ciomadul volcano that, hosting the youngest volcanic activity in Eastern-Central Europe, turned out to have erupted within the past 50 ky.

However, although some basic features of Ciomadul's eruptive history have been clarified since the onset of modern volcanological work (e.g., Szakács and Jánosi, 1989; Szakács and Seghedi, 1989, 1990, 1995; Szakács et al., 1993, 2015), there are still a number of open questions that need to be addressed. These include 1) the structure of the central dome complex that is thought to have been formed during late-stage explosions; 2) the duration and magnitude of volcanism; 3) the types of explosive eruptions (e.g., pyroclastic falls vs pyroclastic density currents; phreatomagmatic/vulcanian vs [sub]plinian) eruptions) along with their source vents (i.e. craters vs lava domes); 4) the areal distribution of pyroclastic units and their potential in providing regional tephrostratigraphic marker horizons; and 5) a detailed tephrostratigraphy including precise dating of individual eruptive events and chemical characterisation of juvenile tephra components (e.g., volcanic glass), for

[1]Official Romanian names, when mentioned at first, are followed by locally used Hungarian names (in brackets), also helpful for the reader to find names on local maps.

correlating Ciomadul fallout tephra in distal sedimentary repositories (e.g., loess and possibly marine sediments).

This paper, focusing on the most recent volcanic evolution of Ciomadul, addresses several of the above listed research questions with a special emphasis on age relationships of the main eruptive stages for the last ~50 ky, which is a highly important and still controversial topic (e.g., Karátson et al., 2013; Harangi et al., 2015; Szakács et al., 2015). Despite the recently accumulated number of age constraints, it is uncertain when the last eruption occurred, this being a crucial piece of information required for assessing volcanic hazards at Ciomadul. For example, Harangi et al. (2015) argued for a "youngest" eruption of 32.6 ka, and a "last major" eruption of 38.9 ka, whereas Szakács et al. (2015) placed the "last eruption" at 27-35 ka, although its deposits were dated at 43 ka by Harangi et al. (2010). Moreover, it is not clear, of what type these eruptions were, which vent(s) they originated from, how they are related to changes in volcano morphology, and how they are preserved in the regional tephrostratigraphic record. Answering these questions has important implications for the Quaternary stratigraphy both in the East Carpathians and also in distal areas (e.g., Constantin et al., 2012; Fitzsimmons et al., 2013; Veres et al., 2013; Anechitei-Deacu et al., 2014).

In our work, we re-evaluate all available published data with an emphasis on radiometric ages of outcropping pyroclastic units (several of them newly identified), and present field observations, grain size analyses and detailed major element glass geochemistry of tephra units. Additionally, we provide new optically stimulated luminescence (OSL) data of proximal and medial/distal sedimentary successions as well as radiocarbon dates from lacustrine sediments from St. Ana and Mohoş craters, in order to constrain tephra accumulation ages. Our results show that the final explosive eruptions of Ciomadul was characterized by at least two closely-following violent explosive stages, of which the

younger, so far unknown activity took place at ~29.6 ka BP, some 2,000 years later than the previously thought latest eruption (i.e. ~31.5 ka: Vinkler et al. 2007, Harangi et al. 2010). The work presented here provides first results of a comprehensive, multi-disciplinary tephrostratigraphic investigation of the evolution of the Ciomadul volcano during the last glacial cycle.

2. Main geologic features and previous research

2.1 Geological and geographical setting

Ciomadul volcano is located at the southernmost tip of the 700 km-long Inner Carpathian volcanic arc, terminating the Călimani (Kelemen)—Gurghiu (Görgényi)—Harghita (Hargita) Miocene to Pleistocene volcanic range of the East Carpathians (Fig. 1; e.g., Seghedi et al., 2004, Pécskay et al., 2006). Forming a massif rather than a central volcano, Ciomadul crosscuts the fold-and-thrust orogenic belt of the East Carpathians that consists mostly of Cretaceous flysch nappes (e.g., Săndulescu, 1988; Fig. 2).

Along the inner part of the East Carpathians, a complex, subduction-related, post-collisional volcanic activity occurred (Mason et al., 1998; Chalot-Prat and Gîrbacea, 2000; Seghedi et al., 2004), showing a time-space along-arc migration in the past ~10 Ma (Pécskay et al., 1995, 2006) and a gradual decrease in magma output with time (Szakács et al., 1993, 2015; Karátson and Timár, 2005). Within this framework, Ciomadul volcano is the site of the youngest activity in the Carpatho-Pannonian Region, still controversially confined either to the past 1 Ma (Szakács et al., 2015) or only to the past 250-200 ka (Karátson et al., 2013; Harangi et al., 2015).

Geographically, Ciomadul is separated from the main volcanic range by the river Olt at Tuşnad (Tusnád) Gorge and emerges at the southern end of the Lower Ciuc (Csíki) Basin (700 m a.s.l., Fig. 1). The volcano comprises a group of typically steep isolated hills, the central and highest amalgamated part (1301 m at Ciomadul Mare [Nagy-Csomád]) of which hosts the twin craters of St. Ana and Mohoş, and a relatively flat summit ridge in the north (Fig. 2). Whereas the peripheral hills commonly show a conical or twin-peaked morphology (Schreiber, 1972) and correspond to individual lava domes consisting of coherent dacite and talus breccias (Szakács and Seghedi, 1995; Karátson et al., 2013; Szakács et al., 2015), the northern ridge towering above the craters is interpreted as a central dome complex truncated by explosive eruptions (Szakács and Seghedi, 1996; Karátson et al., 2013). The rims of the eastern Mohoş crater as well as the southern flanks of St. Ana crater are mostly composed of late-stage pyroclastic deposits. An exception is the Piscul Pietros (Köves Ponk) lava flow, extending from the southern rim of the Mohoş crater (Fig. 2).

Typical rocks of Ciomadul are porphyritic dacites, with a mineral assemblage consisting of plagioclase, amphibole and biotite, occasional clinopyroxene, orthopyroxene, quartz, K-feldspar and olivine, as well as accessory minerals of apatite, titanite, zircon and allanite (Jánosi, 1983; Szakács and Seghedi, 1986; Mason et al., 1996; Kiss et al., 2014). Geochemically, the Ciomadul dacites are representative of the K-rich magmas of the South Harghita volcanic complex enriched in incompatible trace elements (Szakács et al., 1993; Mason et al., 1996). At Ciomadul, these magmas are considered "fairly homogenous" in composition through time by most authors (SiO_2=63-68 wt%; K_2O=3.0-3.5 wt%: Szakács and Seghedi, 1986; Vinkler et al., 2007; Kiss et al., 2014). However, Vinkler et al. (2007) pointed out that the pumiceous pyroclastic sequence exposed at Băile Tuşnad (Tusnádfürdő; locality BTS hereafter; Fig. 3) is more SiO_2-rich and less enriched in incompatible trace elements compared to other pyroclastic and typical lava dome rocks.

The volcanic activity of Ciomadul started at the southern margin of the Lower Ciuc Basin in a fluvio-lacustrine environment (Bulla, 1948; Kristó, 1957; Fielitz and Seghedi, 2004). Drainage of the basin by the present-day river Olt, possibly post-dating the onset of the volcanism, is discussed in Karátson et al. (2013).

At and around Ciomadul, the presence of a still active magma storage system has long been inferred from high heat flux, microseismicity, and intense CO_2 degassing in mofettas (e.g., Vaselli et al., 2002; Szakács et al., 2002). Seismic tomography data support an active crustal magma chamber at depths of 8-20 km (Popa et al., 2012). However, to assess the possibility of future volcanic activity, a detailed chronology of the last eruptions is required.

2.2. Late-stage geochronology — an overview of previous research in a historical context

2.2.1. Qualitative and relative dating

With its "youthful" morphology and gas emanations (mofettas), Ciomadul's relatively young age was already noticed in the late 18th century. It was first von Fichtel (1780), in a book chapter entitled "Ist der siebenbürgische Berg Büdösch ein brennendes Steinkohlenflötz, oder ein Vulkan?" (Is the Büdös Hill in Transylvania a burning coal layer or a volcano?), who argued for the volcanic origin of St. Ana crater, and described sulphurous exhalations of Muntele Puturosu (Büdös Hill, Fig. 2) as products of a "still burning volcano". A similar description was later given by Hauer and Stache (1863). Noticing the "fresh-looking" shape of volcanic landforms, the geomorphologist Cholnoky (1922) argued that "if we did not have the vegetation cover, we could expect the rejuvenation of volcanic eruptions in almost any moment". The young age, however, was contradicted by the contemporary geologist Bányai, who—describing, among others, a key outcrop of a pumiceous unit

(Bányai, 1917) interbedded in a terrestrial sediment sequence at the Fehérmartok locality near the town of Târgu Secuiesc (Kézdivásárhely; locality TGS herafter)—claimed in a conclusive chronological paper (Bányai, 1964) that the exposed tuffs or tuffaceous layers are just reworked deposits of Pliocene age. Soon after, this view was corrected by Peltz (1971) and Rădulescu (1973) on the basis of basin-filling sedimentary relationships, placing the volcanism of Ciomadul to the Mid- or even Late Pleistocene.

2.2.2 Radiometric dating

The Late Quaternary age of Ciomadul was proven unambiguously when radiometric dating begun in the 1980's. The first attempts applied the K-Ar method on whole rock samples and, subordinately, biotite separates from lava rocks to date the Ciomadul lava domes (Casta, 1980; Michailova et al., 1983; Pécskay et al., 1992, 1995). In one of these works, Pécskay et al. (1992) determined an age as young as 0.15 Ma, close to the lower limit of the applied K-Ar method. In addition, Pécskay et al. (1995) obtained an age of 0.5 Ma for a biotite separate from dacitic lithic clasts in the upper pyroclastic-flow deposit of the above-mentioned Băile Tuşnad locality (BTS-1 hereafter, in our division unit 1.5 'E'; Table 1 and 2). However, neither the question of the contribution of inherited crystals (i.e. picked up from older magma), nor methodological problems related to dating various mineral fractions (e.g. biotite, amphibole), have been addressed in detail.

Beginning in the mid-1990's, chronological investigations at Ciomadul have been supplemented by the radiocarbon method. First, Juvigné et al. (1994) used charcoal fragments found in the same BTS-1.5 unit, and obtained a surprisingly young age (10,700±180 ^{14}C yrs BP uncalibrated). However, this age was discarded by radiocarbon re-dating of charcoal from the same unit as well as of the underlying paleosol by Moriya et al. (1995, 1996) and later by

Harangi et al. (2010), pointing out a much older age of ~43 cal ka BP age (see Table 2). Albeit close to the upper limit of radiocarbon dating, this age estimate is ten times younger than the previous K-Ar age of the same pyroclastic unit (i.e. Pécskay et al., 1995). Vinkler et al. (2007) and Harangi et al. (2010) also dated charcoal from another pyroclastic-flow deposit near Bixad (Sepsibükszád, locality denoted as BIX-1 in our paper, see Fig. 3, Table 1), that turned out to be even younger (~31.5 cal ka BP; calibration according to Stuiver and Reimer 2013, see unit code BIX-1.2 in Table 2). At the same time, two preliminary Ar-Ar dates (without analytical data) were presented by Karátson (2007) using biotite separates from pumices of unit BTS-1.5 as well as a massive pyroclastic-flow deposit of the volcano-sedimentary sequence in the P. Rosu (Veres stream) outlet valley of the Mohoş crater (MOH-PR-1 locality hereafter, unit MOH-PR-1.3/1-4 M3). The obtained dates were again older by one order (474 ka and 270 ka, respectively) than the radiocarbon-based age estimates, and can be interpreted as pre-eruptive ages of inherited biotite crystals.

Whereas the above presented radiometric dates verified very young explosive eruptions, the timing of the lava dome activity remained poorly constrained. At first, Karátson et al. (2013) presented morphometric dating results of the Ciomadul lava domes corroborated by preliminary (U-Th)/He ages obtained on zircon crystals. These authors argued for a period of volcanism within the past 200-250 ka, with some dome ages ≤50 ka. A young age was recently confirmed by Harangi et al. (2015) on the basis of disequilibrium-corrected results of (U-Th)/He dating of the Piscul Pietros lava flow. At the same time, Szakács et al. (2015) presented fourteen new K-Ar dates obtained from whole rock samples (in one case a biotite separate) focusing on both the younger and older rocks, partly from the same localities as in Karátson et al. (2013) and Harangi et al. (2015). For the young domes that can be correlated, Szakács et al. (2015) claimed, on average, five to ten times older

eruption ages. Obviously, dating the Ciomadul lava domes—with a focus on eruptive ages rather than mixed (i.e. whole rock samples) or inherited ages—is still a challenging issue.

As for the explosive activity, Harangi et al. (2015) also published (U-Th)/He eruptive ages for five pyroclastic units using zircon crystals from pumices, ranging from 56 to 33 ka, which are highly relevant from the viewpoint of the present paper. The (U-Th)/He ages were calculated as mean values of 3 to 8 dated zircons each (see Table 2 for summary data). Evaluation of the zircon ages obtained by Harangi et al. (2015) with an emphasis of error assessment will be given in Section 5.3 along with other dating results.

In the present work, we target the construction of a "tephra event stratigraphy" with the aim of defining individual eruptions or eruptive phases and their timing. This is a challenging task due to the combination of the general complexity of eruptive activity on explosive lava dome groups similar to Ciomadul (see discussion in Karátson et al. 2013), the poor exposure and preservation conditions of Ciomadul's tephra deposits, and the difficulties of dating methods applied to young volcanic rocks. Therefore, in a first step towards reconstructing the late-stage volcanic history, we focus on the integration of the available proximal and medial/distal sites to establish the most complete tephrostratigraphy possible.

3. Volcanology of pyroclastic successions

In this study, we provide a uniform field description for all previously studied sites and several new localities, supplemented by major element glass geochemistry of pumices and grainsize analyses of tephra deposits for most of the outcrops. Outcrop locality names appearing in the previous literature are sometimes confusing and difficult to identify, especially for an international volcanology usage. Therefore, all exposure names have been merged into a simple and consistent three-letter labelling system, which is easy to understand

in the field and to further develop by adding new sites. For example, as already referred to above, in our system BIX is a locality name, and BIX-1, BIX-2 etc. indicate particular outcrops we describe. The identified pyroclastic units belonging to a given outcrop are labelled in statigraphic order from base to top with increasing numbers (e.g., basal unit BIX-1.1, overlain by unit BIX-1.2, etc.). When describing units, we focused on volcanic or volcanic-sedimentary deposits; nonvolcanic units were distinguished only for important reasons (e.g., OSL dating).

In the following, brief information on all proximal localities are presented along with some key outcrops of medial/distal localities in alphabetical order (Figs. 4-9 and Supplementary Figs. 1-3). To the W and E of Ciomadul, higher terrains may have formed barriers against volcaniclastic deposition and, accordingly, we have found medial-distal outcrops only to the N and S. Further fieldwork in the area is expected to result in identifying new outcrops to be considered in subsequent studies.

In Table 1, geographic coordinates, stratigraphic division, and for most of the described units, the type of major element-based rhyolitic glass composition and granulometry of the pyroclastic components are given, as well as volcanological interpretation of each unit.

3.1. Proximal localities

BTS-1 ("Băile Tuşnad"; ~2 km W of Lake St. Ana and ~1.5 km S of Băile Tuşnad town, roadside quarry along E578/nat. 12 highway, Suppl. Fig. 1). Previous descriptions of the outcrop are found in Teulade (1989), Moriya et al. (1995, 1996), Szakács and Seghedi (1996), Karátson (2007), Vinkler et al. (2007) and Szakács et al. (2015). Main features: The ca. 30 m-long and 12 m-high vertical wall of the abandoned quarry exposes a composite

pyroclastic sequence consisting of at least 3 well-defined pyroclastic units, underlain by a paleosol and overlain by a debris-flow deposit. The paleosol sits on a pyroxene andesite lava breccia (not exposed at present), linked to the neighbouring Pilisça (Piliske) volcano (Szakács and Seghedi, 1995). Units of the outcrop (BTS-1.1 to BTS-1.7) correspond to A-G as reported in Karátson (2007). Description: unit BTS-1.1 ('A', base): ~0.5 m stratified pumice beds (grain size, Ø≤5-8 cm), occasional δ pebbles, all clasts are rounded; unit BTS-1.2 ('B'): 0.3 m sequence of paleosoil divided by beds of small-sized pumice and lithic pebbles; unit BTS-1.3 ('C'): ~4 m un- and weakly stratified, moderately sorted lapilli tuff (sometimes grain-supported) with cm- (≤dm-) sized pumice and occasional δ lithics (Ø≤10-15cm), sandstone xenoliths; unit BTS-1.4 ('D'): 0.6–0.7 m weakly stratified lapilli tuff, cm-sized pumices (in beds), δ lithics (Ø≤8 cm); unit BTS-1.5 ('E') ~4 m unstratified, poorly sorted lapilli tuff/lapilli stone, with pumices Ø≤10 cm and abundant δ lithics Ø≤20-25 cm, occasionally embedded charcoal; unit BTS-1.6 ('F'): ~0.2-0.3 m fine-grained tuffaceous sand; unit BTS-1.7 ('G', top): ~2 m coarse-grained, poorly sorted polymictic breccia.

BIX-1 ("Bixad"; ~2.6 km SE of Lake St. Ana and ~5 km E of Bixad village, roadside exposure on no. 113 community road, Fig. 5A). Main features: First described by Vinkler et al. (2007), the natural, steep outcrop, ca. 10 m high and 20 m wide, reveals stratified beds cut by an epiclastic sequence which is truncated by a pyroclastic-flow deposit (with oblique contact). Due to the steep hillslope above, the latter unit is eroded on top and no upper contact is visible. Description: unit BIX-1.1 (base): ~0.5 m commonly fine-grained, stratified beds of gravel (polimyctic dacite pebbles) with intercalated tuff and tuffaceous sand horizons, truncated by 4 to 5 m coarse-grained, chaotic, polymictic breccia; unit BIX-1.2 (top): 3 to 5 m massive, ungraded, pumiceous tuff breccia with white to light gray pumices of various density, Ø≤30 cm; δ lithic clasts Ø≤10-15 cm; bunches of wood charcoal on the left side.

BIX-2 (~3 km S of Lake St. Ana and ~1 km E of Bixad village, roadside exposure at a bridge on no. 113 community road, Suppl. Fig. 2). Main features: Along the N side of the road, an artificial cut exposes brecciated material of the hillside (previously not described). Description: unit BIX-2: at least 3.5 m thick (lower contact covered), coarse-grained, chaotic, very poorly sorted breccia of uniform, fresh δ clasts up to Ø 1.5 m, with occasional prismatic jointing.

BIX-3 (~4.3 km S of Lake St. Ana and ~1 km S of Bixad village, roadside exposure N of the rivulet of P. Jambor [Zsombor-patak]). Main features: Before reaching the river bed, a local, paved road cut into hillside cliffs reveals pyroclastic flow deposits (previously not described). Description: unit BIX-3: 4 to 5 m massive, ungraded, poorly sorted pumiceous tuff breccia, similar to BIX-1.2, with pumices Ø≤25-30 cm, δ lithic clasts Ø≤10-15 cm.

BIX-4 (~1.2 km SE of Lake St. Ana and ~2.5 km NE of Bixad village, Fig. 5B). Main features: Found on the S hillslopes of St. Ana crater, accessible downhill from the no. 113A community road to St. Ana, this site is a recently incised deep gully with almost vertical walls (firstly reported here), which exposes a series of tuff and breccia units divided by epiclastic layers, soil horizons and colluvium. Due to difficulties in access, only an incomplete description and sampling have been done so far. Some of the units are also observable at nearby gullies. Description: unit BIX-4.1 (base): ~8 m stratified dm-sized beds of light grey tuff with occasional cm-sized pumices, intercalated by tuffaceous sand layers; unit BIX-4.2: overlying interbedded terrestrial sediments, a ~2.5-3 m massive, ungraded, weakly stratified pumiceous tuff breccia, similar to BIX-1.2, with pumices Ø≤30 cm and δ lithic clasts Ø≤10-15 cm; unit BIX-4.3 (top): ~0.5 m fine-grained ash layers with weak stratification, mm-cm sized lithics, occasional pumice.

BOL-1 ("Bolondos Hill"; ~3.4 km E of Lake St. Ana, W slopes of M. Balondoş [Bolondos hill], Fig. 6). Main features: ~0.8 km NE of the junction of no. 113 and 113A

community roads, at the S tip of a large open meadow called Câmpul Lung (Hosszúmező), a 5-7-m deep, ~50 m-long gully has been cut recently in an area of abandoned, infilled pumice pit quarries (active in the second half of the 20th century). A complex, crudely stratified sequence of mostly pyroclastic flow-units is visible. Nearby, at another abandoned pit, named "Covasna-Harghita county border" outcrop by Vinkler et al. (2007), a similar succession has been described (at present, faintly visible due to erosional infill). Description: unit BOL-1.0 (base): ~4 m massive, ungraded, moderately sorted, in the upper ~0.5 m passing into weakly stratified pumiceous lapilli tuff, with pumices and δ lithics Ø≤15 cm; unit BOL-1.1: 0.5 to 1 m sequence of a stratified unit consisting of parallel, slightly undulating 3 lapillistone beds 10-20 cm thick each (with cm-, rarely dm-sized pumices), intercalated by ≤10 cm-thick tuff beds; unit BOL-1.2: 0.3 to 0.4 m massive, ungraded pumiceous tuff breccia, pinching out uphill, with pumices Ø≤15-20 cm, δ lithic clasts Ø≤10-15 cm, and <cm-sized sandstone pebbles from the underlying flysch; unit BOL-1.3: ~0.15 m sandy ash bed with occasional mm-sized pumice fragments; unit BOL-1.4 (top): ~0.2 m 2-3 horizons of well-sorted lapilli tuff and tuff with mm, rarely cm-sized pumice fragments.

MOH-PR-1 ("Mohoş, P. Rosu"; ~2 km NE of Lake St. Ana at Mohoş outlet valley, Fig. 7). Main features: ~100 m far from the edge of Mohoş peat bog, the outlet that once formed a waterfall is now a small gorge, incised ~13 m into loose tephra (in 2015). Along its walls, a spectacular, stratified sequence of thick lower pyroclastic units is exposed, overlain by volcano-sedimentary units that are mostly lacustrine infills of reworked tuffaceous sand and clay. Described shortly by Vinkler et al. (2007) and in detail by Karátson (2007)—in the latter work with a numbering M0 to M40—here only the lower pyroclastic units (M0 to M7) are specified. Samples for OSL dating were taken from unit M5c (OSL sample code MOH-L-1.2) and M34 (MOH-L-1.3), and reported in Table 2. Description: unit MOH-PR-1.0 (M0, base): ~0.9 m moderately-sorted pumiceous lapillistone with cm or dm-sized pumices and δ

lithic clasts; unit MOH-PR-1.1 (M1): ~2 m sequence of parallel, slightly undulating layers consisting of lapillistone beds (with cm, rarely dm-sized pumices) 10-40 cm thick each, divided by stratified ≤10-30 cm-thick tuff / tuffaceous sandy beds; unit MOH-PR-1.2 (M2): ~2.5 m weakly stratified, unsorted, reversely graded tuff breccia with pumice Ø≤15 cm, clasts often broken, δ lithic clasts Ø≤8 cm; the lower two third of the matrix (A) shows limonitization in the matrix in contrast to the upper grayish 0.5 m (B); unit MOH-PR-1.3 (M3A) and unit MOH-PR-1.4 (M3B): 3.5 to 4 m weakly stratified, unsorted, reversely graded tuff breccia, similar to BIX-1.2, with white to light gray pumices of various density, Ø≤25 cm, clasts often broken, and δ lithics Ø≤8 cm; the lower two third of the matrix (A) shows limonitization in the matrix in contrast to the upper greyish 0.5 m (B); (not sampled, M4: ~0.4 m, 20 cm reddish clayey sand with pumice fragments [A] overlain by 20 cm orange and gray pumiceous sand [B]); unit MOH-PR-1.5 (M5): ~0.5 m, 20 cm orange-purple clay (A) overlain by 20 cm well-sorted tuff with cm-sized pumice (B) and 15 cm sandy clay (C); unit MOH-PR-1.6 (M6A): ~0.5 m moderately sorted, ungraded lapilli tuff with cm-sized pumice and δ lithic clasts Ø≤5 cm; unit MOH-PR-1.7 (M6B): ~0.7 m tuffaceous sand passing into reversely graded lapilli tuff with pumice (Ø≤10 cm) and δ lithic clasts (Ø≤5 cm); unit MOH-PR-1.8 (M7A-B): ~0.4 m, 20 cm orange clayey sand (A) and 20 cm pumiceous sand (B); unit MOH-PR-1.9 (M7C, top of described units): ~0.3 m reversely graded lapilli tuff with cm-sized rarely Ø ≤8 cm pumices.

MOH-VM-1 ("Mohoş, Vârful Mohoş": ~2 km NE of Lake St. Ana, Mohoş outlet valley N side, a trail cut ~0.5 km under Vârful Mohoş [Mohos-tető], Suppl. Fig. 3). Main features: The 3-m-high, 10-m-wide outcrop is found where the trail around Mohoş peat bog diverges toward Lăzăreș ti (Lázárfalva) village. The cut exposes at least three pyroclastic units (the uppermost one eroded, and covered by soil) that have not been described so far. Description: unit MOH-PR-1.1 (base): ~0.5 m weakly stratified pumiceous lapilli tuff with

cm-sized pumice, similar to MOH-PR-1.1, lower contact not exposed; unit MOH-VM-1.2: ~2 m massive, ungraded pumiceous tuff breccia with cm-dm sized pumice, poorly exposed; unit MOH-PR-1.3: ~1.5 m massive, unsorted, reversely graded tuff breccia, similar to BIX-1.2, with white to light gray pumices of various density, Ø≤30 cm, δ lithics Ø≤20 cm.

RPSA-1 ("Románpuszta, at road to St. Ana": ~2 km NE of Lake St. Ana, a hillside quarry along the no. 113A community road, with local name Románpuszta, Suppl. Fig. 2). Main features: ~100 m S of the road, a small quarry, changing its shape with time, reveals two pyroclastic units. It was described first by Vinkler et al. (2007), but another pit just along the road was already presented by Szakács and Seghedi (1990) who interpreted it as a pyroclastic surge deposit (possibly equivalent to RPSA-1.1). This latter outcrop has been destroyed since. Description: unit RPSA-1.1 (base): ~1.5 m sequence (lower contact not exposed) of parallel, slightly undulating layers, similar to MOH-PR-1.1. consisting of lapillistone beds each 10-40 cm thick (with up to dm-sized pumices), and intercalated with stratified ≤10-30 cm-thick tuff and tuffaceous sandy beds; unit RPSA-1.2 (top): ~3 m massive, unsorted, reversely graded tuff breccia (upper contact eroded), similar to BIX-1.2, with white to light gray pumices of various density, Ø≤30 cm; δ lithic clasts Ø≤20 cm.

SFA-1 ("St. Ana" crater inner slopes beneath Belvedere outlook point, ~0.8 km NE of Lake St. Ana, Suppl. Fig. 3). The afforested inner slopes of St. Ana crater rarely expose the youngest tephra layers that possibly blanket the landscape. One of the few exposures, a natural outcrop at the foot of pine trees beneath the lookout not described so far, is located ~50 m above the winding no. 113A community road down to St. Ana lake. The relatively small outcrop (~0.7-m high, 10 m-wide) reveals a threefold stratigraphy. Description: unit SFA-1.0 (base): ~0.2 m well-sorted lapilli tuff / lapilli stone; unit SFA-1.1: ~0.2 m fine ash layer; unit SFA-1.2 (top): ~0.3 m moderately sorted lapilli tuff with δ lithic clasts Ø≤2-3 cm; unit SFA-1.3: δ lithic clasts and pumices (Ø≤2-3 cm) collected from unit 1.2.

3.2. Medial-distal localities

TGS-1 ("Târgu Secuiesc": ~21 km SE of Lake St. Ana, an abandoned quarry ~0.5 km N of T. Secuiesc, Fig. 8). Main features: Leaving the town on the no. 113 community road toward Turia (Torja) village ~0.8 km in NE direction, an abandoned sand quarry, shielded by a shooting wall used in the past for military practice, reveals on bottom a thick, fine-grained tuff/tuffaceous sand succession and, in the middle, a prominent pumiceous pyroclastic unit interbedded in loess-derivate and colluvium sediments. The latter unit, already mentioned by Bányai (1917), has been referred to in almost all subsequent literature. Samples for OSL dating were taken from sediments right below (sample code TGS-L-1.1) and above (OSL sample code TGS-L-1.2) unit TGS-1.1. Description: unit TGS-1.0 (base): ~2-3 m thick, stratified tuff and tuffaceous sand sequence with occasional, mm-sized δ lithic clasts, lower contact not exposed; unit TGS-1.1 (top): 0.3 to 0.4 m prominent lapillistone bed with reversely graded pumices, in more detail the lower 10 cm is finer, whereas the upper 20-30 cm is coarser-grained (pumices Ø≤2-5, δ lithics Ø≤1-2 cm).

TUR-1 ("Turia": ~17 km SE of Lake St. Ana, a partly abandoned, partly active quarry ~0.5 km SE of Turia village). Main features: Along the no. 113 community road, the S walls of the quarry exposed a succession of dm- to m-thick beds (previously not described, but in the year 2015 destroyed), consisting of tuffaceous sandy units of mostly laharic origin and a thick package of loess and loessy sand, intercalated by an undulating pumiceous pyroclastic unit. Description: unit TUR-1.1 (base): ~8 m thick stratified tuffaceous sand sequence, possibly with intercalated tuff layers, containing occasional mm to cm-sized pumice fragments and Ø lithic clasts, lower contact not visible; unit TUR-1.2 (top): <10 cm

pumiceous lapillistone bed, in some places discontinuous and undulating due to syn-depositional aeolian reworking, pumices Ø≤3 cm, often broken.

TUR-2 (~11 km SE of Lake St. Ana, an artificial exposure at an abandoned gas pipeline, ~0.5 km W of Turia village, Fig. 9). Main features: Along the no. 113 community road a 8-10 m-high, ~80 m long road cut reveals tuff beds overlain by loess and loessy sand, intercalated again by a pumiceous pyroclastic unit. Samples for OSL dating were taken from the colluvium right beneath the lower tuff unit(OSL sample code TUR-L-1.1) and from between the tuff and the intercalated pumice (OSL sample code TUR-L-1.2). Description: unit TUR-2.1 (base): ~1.5 m crudely stratified tuff and tuffaceous sand sequence with minor cross-bedding, with yellowish-reddish lower contact zone due to remineralisation of organic matter (i.e. grass) and precipitation of Fe- and Mn-oxides; unit TUR-2.2 (top): <10 cm pumiceous lapillistone bed, slightly undulating due to syn-depositional aeolian reworking; pumices Ø≤3-4 cm, often broken.

SNM-1 ("Sânmartin": ~17 km N of Lake St. Ana, an abandoned pit quarry ~0.5 km N of the village of Sânmartin [Csíkszentmárton], Fig. 9). Main features: Beside the E578/nat. 12 highway, in a large pit quarry deepened ~50 m below the ground, the exposed gravelly material of the surrounding alluvial fan reveals an interbedded double layer of pyroclastic-fall deposits (previously not described). Description: unit SNM-1.1 (base): ~15 cm non-stratified, well-sorted, coarse-grained, clast-supported lapilli tuff with abundant, altered, mm-cm sized lithics ± pumice; prominent reddish lower contact zone due to remineralisation of organic matter (i.e. grass) and precipitation of Fe- and Mn-oxides; unit SNM-1.2 (top): ~0.5 m faintly stratified, very well-sorted, fine-grained tuff.

4. Materials and methods

4.1 Grain size analysis, componentry, and pumice density measurements

In order to obtain grain size distribution of the field-described pyroclastic-fall vs PDC-deposits (within the latter we focused on massive pyroclastic-flows), two fresh samples, 1 to 2 kg each, were collected from the selected outcrops (py-fall deposits: BTS-1.3 unit 'C'; TUR-1.2; TUR-2.1 and -2.2; TGS-1.1 upper and lower sub-unit; SNM-1.1 and -1.2; py-flow deposits: BTS-1.5 unit 'E'; BIX-1.2; BOL-1.2; MOH-PR-1.3/1.4 'M3'; MOH-VM-1.3 upper and lower sub-unit; RPSA-1.2 upper and lower sub-unit). At first, a standard, simple sieving procedure was applied to each ~0.5 kg of the samples with phi-scale sieve diameters of 1, 2, 4 and 8 mm. Second, the size of larger clasts (>16, >32 and >64 mm) were determined by taking the average of the two smaller diameters of each clast within phi sized graphic circles. Third, the distribution of the <1 mm fraction, taking small amounts (~1 g) subsequently three times, was determined with laser diffraction particle size analysis in the following way. For five minutes, ultrasonic treatment was applied to complete dispersion, then particle size distribution was measured by laser diffraction (Horiba Partica LA-950 V2, 2013, with 92 individual volume-percentage classes between 10 nm to 3 mm). The three repeated measurements of each sample were taken in order to monitor homogeneity of grain size distribution. To calculate particle size, the refractive index and the imaginary part were assumed to be 1.54 and 0.01, respectively (Eshel et al., 2004; Varga et al., 2015). Out of the three measurements, the distribution was used that showed the best fit of the measured to the theoretical distribution (Horiba, 2008). Finally, the volume-percentage results were merged into five phi particle size classes: 0.5–1.0 mm; 0.25–0.5 mm; 0.125–0.25 mm; 0.0625–0.125 mm; and <0.0625 mm. The mass of each particle size class was calculated on the basis of the total weight of <1 mm fraction and the density of the particles. Density was determined using

a pycnometer (Rowel, 1994). Granulometry results are presented in the standard σφ/Mdφ diagram (see Figs. 5-9 and Suppl. Figs. 1-3 for detailed results, and Fig. 10 for summary).

Several of the described units, in addition to ash-sized particles, contain moderately to highly vesiculated pumiceous clasts. In the characteristic, widespread py-flow unit described above and represented by BIX-1.2, BIX-3, BIX-4.2, MOH-PR-1.3/1.4, MOH-VM-1.3, the pumiceous clasts have various density, easy to detect manually and also by colour difference (lighter pumices are whitish, heavier ones are yellowish grey to grey). In some outcrops, Vinkler et al (2007) referred qualitatively to two density types. To quantify the difference, density measurements of 73 pumiceous clasts from the BIX-1.2 py-flow deposit have been conducted. At first, mass of oven-dry clasts (m_o) were weighted using an analytical balance (mg). Second, measuring cylinders (100 ml ± 0.01 g; 250 ml ± 0.01 g) were filled with distilled water until half of the volume, respectively. Third, the clasts were put into measuring cylinders at 24^{o}C, and the volume of the clasts (v) were determined. Density of the clasts, showing a range from 0.9 to 2.3 (see Fig. 5 and Supplement 1), was calculated on the basis of the ratio of m_o and v (Rowel, 1994).

Apart from the ash and the pumiceous material, for some described units the dark, non-vesiculated, coherent dacite lithic and the non-volcanic (i.e. sedimentary) clasts have also been weighted. On average, 90-95% of the pyroclastic material is pumice, and 5-10% consists of dense lithic clasts. Of the latter, 50-60% is fresh dacite, 30-40% altered dacite, and a few percentages comprise various crustal xenoliths (Fig. 11). Altered dacite lithics have been investigated with Raman spectroscopy, using a HORIBA JobinYvon LabRAM HR instrument at Eötvös University. According to the obtained Raman spectra, the altered brownish surface layer (see Fig. 11) is mostly dominated by magnetite. Of the xenoliths, one type, represented in the BTS units, is a mm–cm-sized, soft, reddish sandstone, whereas

another type, found only in unit BOL-1.2, is a cm-sized micaceous sandstone pebble that is considered a rip-up clast from the underlying flysch by the pyroclastic flow.

4.2 Major element glass geochemistry of tephra units using EPMA

Several representative, fresh pumices were sampled from tephra units from most of the studied proximal and medial/distal sites (see Table 1) for determining the major element composition of juvenile components (volcanic glass shards) by electron probe micro analyses (EPMA). In addition, pyroclastic material from the lowermost part of the Lake St. Ana sediment core and two primary tephra layers from the Mohoş sediment core MOH-2 (Section 4.3) were also analysed. Larger pumices were crushed, and the remaining finer-grained fraction was wet-sieved through 20 µm and 125 µm mesh sieves. Organic-rich samples were treated with a 15% hydrogen peroxide (H_2O_2) solution for several hours, and a 10%-hydrochloric acid was briefly added to samples interbedded within loess and colluvium deposits in order to remove any organic matter and carbonates, respectively. The residual tephra sample was embedded in resin (Araldit©2020, Epofix) and polished thin sections were prepared for EPMA. The major element chemical composition of individual glass shards was obtained by a JEOL-JXA8230 probe at the GFZ German Research Centre for Geosciences in Potsdam. Analytical conditions were set up to a beam voltage of 15 kV, a beam current of 10 nA and beam sizes of 5-10 µm. Exposure times were 20 seconds for the elements Fe, Cl, Mn, Ti, Mg and P as well as 10 seconds for F, Si, Al, K, Ca and Na. Instrumental calibration used natural minerals and the rhyolitic Lipari obsidian glass standard (Hunt and Hill, 1996; Kuehn et al., 2011). Results of glass samples together with the rhyolitic Lipari standard data are reported in Supplement 2. Glass data of individual tephra samples were evaluated in terms of

microcrystal inclusions, then normalized on a water-free basis and juxtaposed in bivariate discrimination diagrams (Fig. 12A-B).

4.3. Radiocarbon dating of the sedimentary infill of the two craters

4.3.1. St. Ana crater

The sedimentary infill of Lake St. Ana was sampled in 2013 using an UWITECH piston corer (http://www.uwitec.at/html/frame.html) equipped with 9 and 11 cm diameter steel and plastic sample chambers. The recovered sediment core SZA-2013 was 17 m long, and the basal sediment consisted of sandy silt and gravel of reworked pumice fragments and dacitic lithics. Pyroclastic components in the lowermost 2 m sediment were very coarse grained (up to 2-3 cm in diameter), indicating that core SZA-2013 reached the bottom of the lacustrine sedimentary succession in the crater.

In order to estimate the age of St. Ana crater formation and the onset of lacustrine sediment accumulation, radiocarbon dates from the lowermost 4 m of core SZA-2013 (Fig. 3, Table 2) were obtained on pollen extracts (44-88 and 88-180 μm fractions) given the lack of plant macrofossils. Radiocarbon measurements were performed in the Hertelendi Laboratory of Environmental Studies at the Institute of Nuclear Research (ATOMKI) in Debrecen, Hungary, using a new MICADAS accelerator mass spectrometer (AMS) with gas ion source interface (Molnár et al., 2013). The obtained ages, calibrated using the IntCal13 calibration curve (Reimer et al., 2013), are given as calibrated radiocarbon years before present (cal yr BP) in Table 2. The pollen extraction method is described in detail in Supplement 3. Only inorganic solvents were used during the sample preparation to avoid contamination by

modern carbon, and special emphasis was placed on the physical separation of the sediment components by involving multiple sieving steps.

4.3.2 Mohoş crater

In order to find an appropriate location for coring the palaeolake sediments of Mohoş crater, Electrical Resistivity Tomography (ERT) measurements were carried out in the crater area in 2012 using the ARES-G Automatic Resistivity system (GF Instruments, Czech Republic). The electrode cable system was four 21 take-out cables spaced every 4 m. When all the four cables were connected, the maximum total length was ~400 m and this could probe to a depth of about 70 m. The multi-electrode gradient array was used for acquiring the data with the Wenner-Alfa protocol. The maximum AB electrode distances were 380 m and 312 m, while the minimum AB electrode distances were 12 m and 24 m, respectively. The length of electric impulses was 0.5 second. The measured data were further inverted using the Res2dinv software to produce 2D resistivity models (Loke and Barker, 1996). In this paper, one resistivity image is shown (Fig. 3) compiled from the eight lines placed radially around the estimated crater interior. Detailed results of the geoelectric survey will be presented elsewhere.

The drillsite of Mohoş crater was positioned along the geoelectric survey line Mohoş-1 at 46°08’21.7’’N, 025°54’15.2’’E (Fig. 3), where the estimated thickness of the low-resistivity fine-grained lake sediments exceeds >70 m. Drilling started from the mire surface and reached down to 30 m depth, and an electric hammer was applied to penetrate the corer into the extremely stiff clayey-silty material underlying the ~10 m thick Holocene peat layer. In the MOH-2 core at 1521.5-1544 cm and 1552-1564 cm composite depth, two primary, coarse grained and decimeter-thick tephra layers, labelled here as RO-1/2/3 and RO-4/5, were

recovered (Fig. 14) which were identified as representing the two youngest pyroclastic deposits (see section 5.2). Dating of the uppermost pyroclastic unit was attempted by two AMS ^{14}C measurements above the tephra layer at 1369-1371 cm (charcoal fragment) and 1519-1521.5 cm (bulk sediment) carried out at the University of Cologne. The samples were pretreated according to Rethemeyer et al. (2013) with the graphite targets measured at the University of Cologne (Table 2). The obtained, conventional radiocarbon ages (Fig. 14) were converted into calendar ages and are reported in cal yr BP using the INTCAL13 calibration curve (Reimer et al., 2013).

4.4. Luminescence dating

Samples for optically stimulated luminescence (OSL) dating were collected by hammering 20 cm-long stainless steel cylinders into freshly cleaned sediment sections at a number of proximal and medial/distal outcrops (Table 1). Loess and loess-derivate terrestrial sediment samples were taken below and above selected tephra units as given in Sections 3.1 and 3.2. The sediment from the central part of the each tube was processed in the luminescence dating laboratories of Babeş-Bolyai University (Cluj-Napoca, Romania) and Eötvös Loránd University (Budapest, Hungary), respectively, under low intensity red light to extract fine-grained (4-11 μm) quartz. The samples were treated with hydrochloric acid (HCl; concentration of 10% followed by 35%) for calcium carbonate removal followed by a two-days hydrogen peroxide (H_2O_2; concentration of 30%) treatment in order to remove organic matter. Extraction of quartz grains of 4-11 μm from the fraction less than 63 μm followed conventional procedures for sample preparation (Frechen et al., 1996; Lang et al., 1996). After isolating the fraction less than 11 μm by settling in Atterberg cylinders according to Stokes' law, the polymineral fraction has been etched with 35% hexafluorosilicic acid

(H_2SiF_6) for 10 days to obtain pure quartz. Subsequently, centrifugation in distilled water has been carried out to remove the grains <4 μm. Aliquots were made by pipetting a 1-ml suspension of the fine grains (2 mg of grains/1 ml acetone) onto each aluminium discs. The infrared stimulated luminescence (IRSL) response to a large regenerative β-dose measured at 60°C (IR depletion test) has been used to evaluate the purity of the quartz extracts. A significant sensitivity to infrared stimulation accounts for an IR depletion ratio deviating more than 10% from unity.

For annual dose calculation, radionuclide specific activities were determined through high-resolution gamma-ray, and the dose rates were calculated using conversion factors published by Adamiec and Aitken (1998). The information relevant for annual dose calculation is given in Supplement 4. Luminescence measurements were performed using standard Risø TL/OSL-DA-20 reader at Babeş-Bolyai University for four samples (TUR-L-1.1, -1.2 and TGS-L-1.1 and -1.2), and at Eötvös University for two samples (MOH-L-1.2 and -1.3). Both readers are equipped with both blue and infrared LEDs emitting at 470±30 nm and 875±80 nm, respectively. The emitted luminescence signals were detected by EMI 9235QA photomultiplier tube through a 7.5 mm thick Hoya U-340 UV filter. Irradiations were carried out using the incorporated ^{90}Sr-^{90}Y radioactive source that was calibrated against gamma dosed calibration quartz supplied by Risø National Laboratory. A dose rate of 0.120 Gy/s was derived for the fine quartz grains mounted on aluminium discs in the laboratory of Babes-Bolyai University, while a dose rate of 0.072 Gy/s was calculated for the fine quartz grains mounted on stainless steel cups in the laboratory of Eötvös University. Equivalent doses were obtained using the Single Aliquot Regenerative Dose (SAR) protocol (Murray and Wintle, 2000; Murray and Wintle, 2003; Wintle and Murray, 2006) (see Supplement 4 for a detailed description of the protocol). The average equivalent doses and the information relevant for optical ages and uncertainty calculation are summarized in Supplement 4.

5. Results and discussion

As a major result of our analysis, we propose a general threefold stratigraphy for the Ciomadul pyroclastic units. A scheme of three main groups, which represent subsequent time slices of eruptive stages or closely spaced eruptions, are shown in Fig. 4. Whereas most sites that belong to the first two groups have been studied or mentioned in the literature, those of the proposed third group are described for the first time in this work.

The earliest explosive eruptions are grouped into the so-called EPPA stage ("Early Phreatomagmatic + Plinian Activity"). Respective pyroclastic deposits of the sites studied in this paper include units TUR-1.1, TUR-2.1, TGS-1.0, BIX-1.1, BIX-4.1, SNM-1.1 as phreatomagmatic units, and BTS-1.3 and BTS-1.5 as plinian units.

The next eruptions are grouped into the so-called MPA stage ("Middle Plinian Activity") and encompass units TGS-1.1, TUR-1.2 and TUR-2.2, MOH-PR-1.0 to MOH-PR-1.5, MOH-VM-1, BIX-1.2, BIX-3, BIX-4.2, BOL-1.0 to BOL-1.3, RPSA-1.1 and RSPA-1.2, and MOH-2 core tephra sample RO-4/5.

The latest eruptions fall into the so-called LSPA stage ("Latest St. Ana Phreatomagmatic Activity"). The sites included here are units BOL-1.4, SFA-1.0 to SFA-1.3, BIX-4.3; SZA2013 core 1605–1612 cm depth; and MOH-2 core tephra sample RO-1/2/3.

In the following sections, volcanological considerations, then geochemical and finally radiometric constraints on the three stages are given.

5.1. Types of volcanic eruptions, and constraints on vent area

Pyroclastic deposits around Ciomadul crop out in only a limited number, but after interpreting and correlating the described units (Table 1, Fig. 4), the exposures give a clue to decipher the eruptive history. In our work, focusing on all known proximal, and some of the medial/distal outcrops, we have documented the characteristics of pyroclastic density currents (PDCs) and pyroclastic falls, from both magmatic and phreatomagmatic explosive activity (Table 1). Within the PDCs, pumiceous pyroclastic-flow deposits are the most abundant.

Analyzing the grain size characteristics of the pyroclastic-fall and -flow deposits, all of them plot in the respective field of the σφ/Mdφ diagram (Fig. 10). The pyroclastic-fall deposits, which are less preserved, are commonly well- or very well-sorted, typically with 40% or even 60% of the total clast population falling within one phi unit interval. In contrast, pyroclastic-flow deposits are poorly sorted, with each phi unit interval comprising only ≤20% of the clast population.

5.1.1. Pyroclastic density current deposits

The more widespread PDC deposits are mostly poorly sorted massive lapilli tuffs (BIX-1.2, BOL-1.0 and BOL-1.2, BTS-1.5, MOH-VM-1.2 and MOH-VM-1.3, MOH-PR-1.2 and MOH-PR-1.3/1.4 'M3', and RPSA-1.2) interpreted as pyroclastic-flow (dense, massive PDC) deposits, and partly better sorted tuff/lapilli tuff sequences (BOL-1.1, MOH-PR-1.1, MOH-VM-1.1 and RPSA-1.1) interpreted as pyroclastic-surge (dilute PDC) deposits possibly intercalated by pyroclastic-fall units. Notably, RPSA-1.2, which was previously described as pyroclastic fall by Vinkler et al., 2007, is defined now as a pyroclastic-flow deposit.

The most prominent PDC type that we correlate over the S and E slopes of Ciomadul (cf. Karátson, 2007) is a 3-5 m thick pyroclastic-flow unit (BOL-1.2; MOH-PR-1.2 and MOH-PR-1.3/1.4; MOH-VM-1.2 and MOH-VM-1.3; RSPA-1.2) thickening toward distal

areas, except for unit BOL-1.2 which stretches on an uphill position in elevated flysch terrain. Pyroclastic-surge deposits of BOL-1.1, MOH-PR-1.1, MOH-VM-1.1 and RPSA-1.1 are interpreted as preceding the massive pyroclastic flows, which always overlie them. Except for unit BTS-1.5, the described massive pyroclastic-flow deposits display abundant lapilli- to block-sized pumiceous clasts with various densities, most obvious for BIX-1.2 and also observable for RPSA 1.2, MOH-VM-1.3, MOH-PR-1.3/1.4 M3 and BOL-1.2. BTS-1.5 also contains pumice but with different glass chemistry (see section 5.2), whereas BIX-2 does not contain any pumice.

From the granulometric point of view, the correlated, massive pyroclastic-flow deposits are very coarse-grained with respect to the worldwide average: within the common pyroclastic-flow area that was defined by Walker (1971) they plot in or around the block-and-ash flow quadrangle of the σφ/Mdφ diagram as suggested by Freundt et al. (1999). Although worldwide comparisons of grainsize characteristics of single block-and-ash flow events are rare, data from two well-known eruptions are also plotted in Fig. 10: the deposits of the 1886 AD Kaharoa eruptive episode of the Tarawera domes (Hanenkamp, 2011) and those resulted from the 2010 AD Merapi dome destruction (Charbonnier et al., 2013). Whereas the majority of the Merapi 2010 and the Kaharoa 1886 deposits fall in the block-and-ash flow quadrangle, the Ciomadul data, although the median diameter is similar to the two cited examples, show slightly better sorting.

The peculiar granulometry along with the variance in clast density of Ciomadul's pumiceous pyroclastic-flow deposits may be explained by the eruption mechanism. Namely, instead of the common, gravity-driven lava dome collapse-generated block-and-ash flows (e.g., at Merapi 2006: Charbonnier and Gertisser [2008], which can be envisaged e.g. for the pumice-free BIX-2 deposit), we propose a more explosive lava dome disruption. This is supported by the measured light to heavy clasts of BIX-1.2 and related pyroclastic-flow

deposits that exhibit a wide range of densities from 0.9 to 2.3 g/cm^3 (the average being 1.6). The density distribution of the clasts is slightly positively skewed (i. e. it deviates from normal) due to the presence of some heavier clasts (2.2-2.3 g/cm^3); one test measurement on a dark, small-sized dacite lithic clast, characteristic of all studied PDC deposits (Fig. 11), yielded a lava-like density (2.5 g/cm^3). Such a wide spectrum points to an origin of a lava dome with an outer carapace and an inner part of variably vesiculated dome material.

Highly explosive lava dome collapses have already been documented at Soufrière Hills, Montserrat, 1997 (Druitt et al. 2002), Merapi, Java, 2010 (Komorowski et al., 2013), Kelud, Java, 2014 (Maeno et al., 2015), and possibly El Chicón, 1982 (Macías et al., 2008). In these cases, pyroclastic flows do not only result from the collapse of the dome, but also from a sustained or periodical vulcanian column collapse producing pumiceous flows (e.g. at Merapi, 2010: Komorowski et al., 2013). At Ciomadul, the observed clast variance of the studied proximal pyroclastic-flow deposits is associated with a distinct geochemistry (see Section 5.2), with one exception again, BTS-1.5 unit 'E', which is a pumiceous pyroclastic-flow deposit, too, but interpreted as having originated from a (sub)plinian column collapse (see Seection 5.1.2 and Szakács et al., 2015). On this basis (except locality BTS-1), we correlate the described proximal pumiceous block-and-ash flow deposits and suggest them to belong to a single eruptive event within the Middle Plinian Activity (MPA). Their correlation is also suggested by field relationships, as all studied units crop out in the same relative level high in the stratigraphy.

As for the eruption scenario of the outlined explosive dome collapse, occasional explosions may have produced pyroclastic surges/flows and minor falls (e.g., MOH-PR-1.1, BOL-1.1, RPSA-1.1). This was followed by explosive dome collapse and/or vulcanian fountain collapse, producing lobes of pumiceous pyroclastic flows (e.g., BIX-1.2, BOL-1.2, RPSA-1.2), and occasionally resulting in subsequent flow events (e.g., MOH-PR-1.2 and

1.3/1.4). The BIX-2 pumice-free block-and-ash flow (Suppl. Fig. 2) may represent another but temporally closely-related dome collapse. The proximal setting of all these deposits, their stratigraphic position, and location around the twin-crater area, imply a vent at or near Lake St. Ana.

5.1.2. Pyroclastic-fall deposits

Ciomadul's pyroclastic-fall deposits can be divided into two: group a): proximal (BTS-1.3 'C') and medial/distal deposits (TUR-1.2, TUR-2.2, TGS-1.1 lower and upper part) containing well-sorted pumice clasts with a median diameter of -2 to -1 phi; and group b): proximal (BOL-1.4, BIX-4.3) and medial/distal deposits (SNM-1.1, SNM-1.2, TUR-1.1 and TUR-2.1) containing no pumice but ash- to lapilli-sized lithics with a median diameter of 0 to 2 phi.

Group a). Except for unit BTS-1.3, this group has a similar componentry: whitish, light pumices and dark, dense lithics, the latter being apparently identical to those in the widespread pumiceous block-and-ash flows described above (Fig. 11). Moreover, although the light pumices seem slightly different from those in the pumiceous block-and-ash flow deposits, there is an obvious, strong geochemical relationship (see Section 5.2), so only the vesicularity and colour make the difference. On this basis, except BTS-1.3 'C', we interpret the pumiceous pyroclastic-fall deposits as related to the same highly explosive event at the St. Ana vent area depicted above. For the locality first mentioned in the literature, we outline an eruption called "TGS" (Târgu Secuiesc) as part of the MPA. In our view, during this bi-phase eruption, the above-inferred explosive dome collapse / fountain collapse may have been followed—perhaps similar to the 2014 eruption of Kelud volcano—by a plinian column

yielding pumice fall to as far as 21 km to the SE (and likely even farther). Age relationships of the proposed contemporaneity are discussed in Section 5.3.

Unfortunately, the preservation of the TGS pumice-fall deposits is poor, and volume estimation is impossible at this stage of knowledge. The pumice was deposited under the cold and dry climate of the last glacial period with loess formation, often on steep slopes, and has been preserved only in a few places. For example, at the TUR-1 and TUR-2 localities, the pumice beds, although closer to the vent than TGS, are thinner and undulating (Fig. 9), possibly reflecting coeval wind erosion; in all localities, rip-up pumice fragments in overlying loess are frequent. The TGS-type fallout pumice is also identified from the Mohoş core sedimentary sequence (described as tephra bed RO-4/5).

BTS-1.3 'C' is also interpreted by most authors as a plinian/subplinian fall deposit, slightly reworked on the steep W slope of Ciomadul (e.g., Szakács and Seghedi, 1996; Szakács et al., 2015). Since, despite mapping the proximal area of the volcano, this is the only outcrop of the deposit identified so far, the peculiarities of the related explosive eruption—referred hereafter as to the BTS eruption—are difficult to assess. According to the geochemical results, we can infer distinct glass chemistry for BTS-1.3 'C' (as well as for the subsequent pyroclastic-flow unit BTS-1.5 'E') compared to the tephras from the proposed TGS eruption (section 5.2); moreover the BTS eruption is older (section 5.3). The proximity with respect to the St. Ana crater (i.e. on its W slope) implies a vent again at or around Lake St. Ana, although venting from the Mohoş crater cannot be completely ruled out either.

Group b). Whereas the above-mentioned pyroclastic-fall deposits stem from magmatic explosions, there are also widespread phreatomagmatic units around the volcano. The exemplary type is unit TUR-2.1 in a medial/distal location, which is a ~1.5 m tuff sequence of pyroclastic fall and surge deposits as well as tuffaceous sand, deposited possibly in the peripheral part of a valley or basin. The yellowish-reddish lower contact zone (also

observable at the SNM locality in the N), that likely formed by precipitation of Fe- and Mn-oxides as a result of remineralization of palaeo-vegetation, reflects fast burial by the tuff. Compared to TUR-2.1, more significant reworking is observed at the more distal unit TUR-1.1, which is exposed on a wide palaeovalley bottom. Here, the tuffaceous beds are significantly thicker with claystone matrix, and are inferred as having been deposited from successive lahars. For these pumice-free successions that contain abundant fine ash and small-sized lithics and have a characteristic glass geochemistry (see section 5.2), we suggest an origin from phretomagmatic eruptions. Syn-eruptive laharic and fluvial reworking of the tuffs is frequently observed. As introduced above, we group these deposits into the EPPA (Early Phreatomagmatic and Plinian Activity), and the peculiar eruptive phase represented at locality TUR-2 is referred to as "Turia eruptions" (for age relationships, see Section 5.3).

The vent area during the EPPA stage, as already proposed by many authors (see discussion in Szakács et al., 2015), could have been the Mohoş crater that overlies groundwater-rich carbonate flysch. However, we argue that the related pyroclastic deposits do not crop out at the Mohoş crater rim (as suggested by e.g. Szakács et al., 2015, or Harangi et al., 2015), because deposits from the younger eruptions of St. Ana covered the early products (cf. localities RPSA-1 or MOH-VM-1). Notably, at locality MOH-PR-1 (i.e. the most complete succession cropping out near the crater rim in the outlet gorge), no early tuffs are exposed even in the lowermost part of the succession. Closest to the vent, the EPPA pyroclastic units were identified only in the bottom succession of the BIX-4 gully. In medial/distal settings, the EPPA tuffs and reworked tuffs are always found in the lowest stratigraphic position (e.g., TGS-1.0, BIX-4.1, SNM-1). A number of other exposures around the volcano, falling probably into EPPA, are subject to future studies.

Surprisingly, above the widespread, easy-to-recognize MPA pyroclastic units, we discovered other phreatomagmatic pyroclastic-fall units that have not been described before.

In fact, these thin (dm-sized) layers are not always obvious in the stratigraphy. The deposits, which show similar characteristics to group b), contain lapilli to ash and rarely pumice fragments, and are reworked in some places (e.g., sandy ash); hence, glass geochemistry is an important tool for identification. The described units belonging to this group comprise BIX-4.3, BOL-1.4, SFA-1 (all units), and possibly MOH-PR-1.6 'M6A'. Moreover, these deposits are identified in both crater lake successions; in the highest stratigraphic level of the Mohoş MOH-2 core (tephra beds RO-1/2/3), and as redeposited pyroclastic layers in the lowermost part of the St. Ana (SZA-2013) core. Around the twin-crater region, units BIX-4.3 and BOL-1.4 are the uppermost, thin tuff or tuffaceous layers on top of complex volcanic-sedimentary sequences, whereas the SFA units drape the inner slopes (below recent soil) of St. Ana crater.

Given the typically fine grain size of these deposits even in proximal settings with no or minor vesiculated juvenile clasts (i.e. pumice), we infer phreatomagmatic explosions originating from an open vent (with no pyroclastic-flow counterparts). As introduced above, these units—which are the youngest products of Ciomadul—are collectively referred to as LSPA (Latest St. Ana Phreatomagmatic Activity). The vent area, on the basis of stratigraphy, field relationships as well as age constraints (Section 5.3), should have been St. Ana crater that may have taken its final shape by this latest eruption.

5.2. Geochemical discrimination and correlation of pyroclastic units

Major element glass compositions of selected proximal and medial-distal tephras reveal three distinct rhyolitic populations (Fig. 12A-B). Pumice clasts of all three types are characterized by a highly to medium vesicular groundmass that is often dominated by a microlite assemblage of plagioclase (Fig. 13), pyroxene and Fe-Ti oxides. Therefore, a

thorough data evaluation was required to avoid misinterpretations based on crystal contamination effects on groundmass glass composition.

One type of glass population, typical of the pyroclastic deposits termed above as "EPPA", is characterised by a heterogeneous, highly evolved rhyolitic composition (~75.2–79.8 wt% SiO_2, 11.3–14.3 wt% Al_2O_3; normalized data) with diagnostic low and variable FeO_{total} (~0.4–0.9 wt%) and CaO contents (~0.3–1.2 wt%). Glass compositions of units BIX-1.1, TUR-2.2, TUR-1.2 and TGS-1.0, i.e. the lowermost units in medial-distal localities SE of Sf. Ana, unit SNM-1.1 from a distal site in the N (Fig. 12A), as well as the slightly less evolved and rather homogenous proximal sites of BTS-1.3 (unit 'C') and BTS-1.5 (unit 'E') (Fig. 12B), are characterised best by this composition.

Tephra units related to MPA show a different type of rhyolitic glass population that is less evolved with lower SiO_2 values of 70.2–74.5 wt% and higher Al_2O_3 (14.3–17.3 wt%), FeO_{total} (0.8–1.8 wt%) and CaO (0.8–2.1 wt%) concentrations compared to EPPA deposits. MPA-type compositions are characteristic for proximal and medial-distal units BIX-1.2, RPSA-1.1, RPSA-1.2, BOL-1.1, BOL-1.2, and MOH-PR-1.1 (M1), MOH-PR-1.2 (M2), MOH-PR-1.3 (M3A) and MOH-PR-1.4 (M3B) (Figs. 12A-B). There are no obvious chemical differences visible between lower pumice fall/surge and upper pumiceous block-and-ash flow units (e.g., samples RPSA-1.1 and RPSA-1.2, respectively; Fig. 12B). A MPA-type composition is also clearly identified in the Mohoş palaeolacustrine sequence as a 12 cm-thick, reversely graded pumice level (sample RO-4/5, interpreted as material fed by the peculiar eruption of TGS-pyroclastic fall or flow). In the distal area, MPA composition is represented in the upper tephra unit at the Târgu Secuiesc (TGS-1.1) and Turia outcrops (samples TUR-1.2 and TUR-2.2; Fig. 12A).

The third, intermediate glass population shows a heterogeneous, slightly less evolved rhyolitic composition compared to the oldest EPPA-type tephra units, with SiO_2

concentrations of 72.8–78.8 wt%, and slightly higher Al_2O_3 (12.0–15.4 wt%), CaO (0.4–1.2 wt%) and FeO_{total} (0.2–1.6 wt%) values. This composition is related to the youngest pyroclastic deposits in proximal and medial localities (i.e. SFA-1.1, SFA-1.2, SFA-1.3, MOH-PR-1.6 M6, BOL-1.4) and, as introduced in Section 5.1, referred to as LSPA. It correlates well with the uppermost, ~22.5 cm thick tephra layer in the Mohoş palaeolacustrine sequence (sample RO-1/2/3: Fig. 12B). The LSPA-type is also diagnostic for the redeposited pyroclastic levels from the basal part of the Lake St. Ana sediment core (sample SZA-2013 from 1605 to 1612 cm depth; Fig. 12A).

The three glass compositions indicate a clear compositional trend of matrix glass from the highly evolved phreatomagmatic products (EPPA tephras) followed by the less evolved MPA pyroclastics to finally the slightly more evolved tephras of LSPA, the latter forming a group that falls compositionally in between the older eruption products. Bulk rock and detailed trace element glass analyses as well as petrological investigations are in progress to provide insights into the pre-eruptive magmatic processes preceding the last explosive period of Ciomadul, and to further aid a more detailed correlation of Ciomadul tephra units.

5.3. Assessment of radiometric data

The succession of Ciomadul's explosive eruptions, constrained by the interpretation of volcanic stratigraphy and major elements glass geochemistry, can be put in a chronological context by critically evaluating the radiometric data (Table 2). Various types of uncertainties and errors can be attached to the applied dating methods [i.e. radiocarbon, luminescence, zircon (U-Th)/He] of Ciomadul's pyroclastic rocks; however, we attempt to constrain the most likely time frame for individual volcanic units/eruptions identified in our work. The

discussion is based on the new and previously published age constraints with respect to our threefold stratigraphic scheme.

5.3.1. Timing of the EPPA eruptions

As mentioned in the introduction, dating of Ciomadul's lava dome rocks is still a challenging issue. A young age of <50 ka for at least one lava flow (Piscul Pietros) has been pointed out by (U-Th)/He dating on zircon grains (Karátson et al., 2013; Harangi et al., 2015) in contrast to a K-Ar date obtained from a biotite separate of the same rock that yielded 0.29 Ma (Szakács et al., 2015). Although this problem needs further investigation, we propose that the final lava dome formation of Ciomadul begun more or less contemporaneously with the explosive activity at ca. 50 ka (Harangi et al., 2015; Karátson et al., 2013; Szakács et al., 2015).

On the basis of our stratigraphic framework, the first explosive eruptions occurred during the EPPA stage and produced commonly phreatomagmatic sequences. Within the EPPA stage, we distinguish a phase called "Turia eruptions", represented by units TUR-2.1 and SNM-1, that is newly dated at the TUR-2 locality by the OSL method on fine quartz grains from underlying colluvium at 51.0±4.8 ka. This proposed age is the oldest known so far for Ciomadul's explosive activity, apart from a controversial 55.9 ka age obtained by Harangi et al. (2015) (see discussion below). We emphasize that the phreatomagmatic deposits of EPPA are widespread, being recognized both proximally (e.g., units BIX-1.1, BIX-4.1) and medially-distally either to the S (units TUR-1.1, TUR-2.1, TGS-1.0) or to the N (SNM-1 locality) of Ciomadul; further geochronological studies are required to refine their succession.

Another, particular explosive phase that we distinguish within the EPPA stage is the bi-phase plinian "BTS" eruption, which produced a thick pyroclastic-fall and -flow sequence, identified only at Băile Tuşnad so far. Szakács et al. (2015) proposed the collapse of a plinian column and subsequent pyroclastic flows after a short phreatomagmatic event, which is a likely scenario, also supported by our field observations, granulometric data and major element glass composition. Based on radiocarbon dating of embedded charcoal, the age of the upper pyroclastic-flow unit BTS-1.5 is ≥40 ka (Moriya et al., 1995) and 42,827±1586 cal yr BP (Harangi et al., 2010, recalibrated as mean age with a 2σ error range according to Stuiver and Reimer, 2013, Table 2). A 43 ka age is in accordance with dating the paleosol underlying the lower pyroclastic-fall unit BTS-1.3 to ≥41 or ≥45 ka (Moriya et al., 1996, Table 2). Notably, all these radiocarbon ages should be considered as minimum values as they are close to the upper limit of the radiocarbon method.

For the lower unit of BTS-1.3, Harangi et al. (2015) obtained a mean 50.3 ka age using the zircon (U-Th)/He method (Table 2), i.e. 7 ka older than the likely coeval upper unit radiocarbon dated at ~43 cal ka BP. However, the individual zircon ages (of 8 dated grains) show a big scatter from ca. 64 to 43 ka, which Harangi et al. (2015) explained as intra-crystal zonation (i.e. heterogenous distribution of U and Th within individual crystals). This problem is to be clarified by further dating approaches, e.g. on a larger number of zircon grains.

Despite the uncertainties of the available radiocarbon and zircon dates, the time frame of the EPPA stage is relatively well constrained within the approximately 50-45 ka period. Further studies are required to clarify the more precise chronology as well as the factors behind the phreatomagmatic vs plinian phases during this stage.

5.3.2. Timing of the MPA eruptions

After the explosive BTS, and the effusive eruption of Piscul Pietros (dated at ~42.9 ka by Harangi et al., 2015), a quiescent period begun.

The next explosive activity we identify is the MPA stage. In particular, we define a bi-phased eruption called TGS. As suggested in section 5.1, during this eruption—subsequent to a preceding lava dome growth at or near the "Proto" St. Ana crater—an explosive dome collapse/vulcanian fountain collapse and associated plinian pumice fall took place. One of the units which we propose to belong to this eruption is the BIX-1.2 pumiceous block-and-ash flow deposit, radiocarbon dated by Vinkler et al. (2007) and Harangi et al. (2010) to a mean ^{14}C age of 31,510 cal yr BP (Table 2).

Zircon (U-Th)/He dating of the same deposit yielded a roughly concordant 32.6±1.0 ka age, with individual ages scattering between ca. 28 and 42 ka (Harangi et al., 2015; Table 2). Another unit, MOH-PR-1.3, which we also correlate with the TGS eruptive phase based on granulometry and glass chemistry data, was zircon (U-Th)/He dated at 34.0±1.0 ka (with similar individual zircon age range from ca. 30 to 42 ka) by Harangi et al. (2015). If we consider the errors given by Harangi et al. (2015) as 1 sigma (σ) and calculate the weighted average of the individual zircon grains using the mean square weighted deviation method (Table 2), the results are 32.6 and 32.7 ka, respectively. This re-calculation calls attention again that analysing relatively few grains may result in larger errors than given in Harangi et al. (2015), so simply considering the mean of the zircon ages as eruptive ages can be misleading. In this view, the conclusion of Harangi et al. (2015) on two subsequent eruptions (with 34 and 32.6 ka) seems unsupported; instead, we suggest that they represent the same TGS phase as shown by the same stratigraphic position, matching componentry, and identical glass composition, with a likely eruptive age of ~31.5 cal ka BP. Notably, this age, as well as the zircon ages, is roughly concordant with the 33.9±2.2 ka OSL date obtained in this study on an overlying sandy clay of MOH-PR-1 'M5C' (see Table 2, Fig. 7).

Another MPA-related unit, BOL-1.0 (Fig. 6), was dated by Harangi et al. (2015) at a mean zircon age of 55.9 ka (with an age scatter of individual zircon grains between ca. 70 and 49 ka), which implies an EPPA age. However, according to field studies, unit BOL-1.0, which is a pyroclastic-flow deposit, passes upward to the stratified BOL-1.1 unit without erosional discordance, and a similar stratigraphic sequence is pointed out for the MOH-PR-1 and partly the RPSA-1 lower units (see Figs. 6-7 and Suppl. Fig. 2). Identical MPA-type glass geochemistry for all these units has been determined (see Table 1, Section 5.2). This way, we can exclude a scenario of a preceding EPPA eruption that shows a likewise MPA glass chemical composition, and suggest a sampling or dating issue for the, in our view, apparently too old zircon age reported in Harangi et al. (2015).

In Section 5.1, we already argued for the contemporaneity of the TGS-1.1 pumice fallout with the widespread pumiceous block-and-ash flow event, supported by identical MPA-type glass geochemistry (Section 5.2). However, radiometric dating of the TGS plinian event —as a possible closing phase of the MPA stage is controversial. Harangi et al. (2015) published a (U-Th)/He zircon age of 38.9 ka, calculated from 3 grains (ca. 37 to 44 ka) after excluding outliers (ca. 75 to 137 ka: Table 2). Harangi et al. (2015) considered the latter as crystals from older deposit; however, such old explosive eruptions are unsupported by field data so far. The 38.9 ka age seemed to be confirmed by additional post-infrared-infrared stimulated luminescence (pIRIR) dating on feldspar from the TGS-1.1 under- and overlying loess-derivate sediments, yielding ages of 43.3±3.0 ka and 35.9±2.9 ka, respectively (Table 2). However, our repeated dating of the same loess-derivate deposits by OSL on fine quartz grains from samples immediately bracketing the TGS-1.1 pumice fallout has now given much younger ages of 30.7±3.0 ka and 24.1±2.3 ka, respectively, which allows the interpretation that the pumice fall occurred coevally (i.e. ~31.5 ka) with the TGS pumiceous pyroclastic flows (e.g., BIX-1.2, MOH-PR-1.3/1.4, BOL-1.2). Notably, another new OSL age of

36.3±3.3 ka obtained 35 cm below unit TUR-2.2 (i.e. the same pumice fallout as TGS-1.1: Fig. 9) is also in agreement with such a younger age relationship.

We already assessed the apparent over-estimation of the mean zircon ages as eruptive ages, in this case based only on 3 grains. As for the pre-eruption pIRIR dating, the too old age obtained by Harangi et al. (2015)—as demonstrated in Fig. 8—may be due to the fact that the sample was collected several tens of centimeters below unit TGS-1.1. Their upper age constraint (which seems to be also too old, i.e. 35.9 ka; sample taken well above the upper boundary of TGS-1.1, see Fig. 8, Harangi et al., 2015) cannot be explained at this stage; it is, however, common that pIRIR ages of such young sediments should be viewed with caution (e.g., Buylaert et al., 2011).

Overall, given the support from various lines of evidence, we maintain to propose that the TGS pumice fallout was coeval with the TGS pyroclastic flows, forming one of the most important eruptive phases within MPA, and is therefore significantly (~7,000 years) younger than claimed by Harangi et al. (2015).

5.3.3. Timing of the LSPA eruptions

In Section 5.1, we presented evidence that the eruptive activity at Ciomadul did not terminate with the MPA stage: the last activity produced the widespread LSPA phreatomagmatic deposits.

We have obtained radiocarbon ages to constrain the timing of LSPA (Table 2). A young age for the St. Ana crater is supported by radiocarbon dating the bottom sediments of the crater infill. The oldest ages determined from the cores SZA-2010 and SZA-2013 on the deepest sediments, respectively, are 25,946±303 cal yr BP (at 1682 cm depth, Karátson et al., 2013) and 27,180±462 cal yr BP (at 2032 cm including 6 m water depth, this study). The new

radiocarbon age from core SZA2013, measured on pollen extracts recovered from fragmented, rocky debris, indicates that the drilling most likely reached the lowermost dateable part of the lacustrine succession, that corresponds to the onset of rapid crater infilling (i.e. loose material washed in from the crater slopes before afforestation).

Another, perhaps more significant evidence derives from dating the Mohoș MOH-2 core, which yielded a 27,762±625 cal yr BP age for the lacustrine sediments at 1369-1371 cm depth, and 29,597±610 cal yr BP age for the sediments directly overlying the uppermost tephra in the core, i.e. the RO-1/2/3 unit, at 1519-1521.5 cm depth. Tephra unit RO-1/2/3 has been correlated with the LPSA eruption based on its glass chemical composition, and it is underlain by the MPA-type tephra RO-4/5 (see Fig. 14). This way, we suggest the ~29.6 ka BP date as a reliable age constraint of the final eruption at Ciomadul.

As for the distribution of the Ciomadul tephras, based on the presented data on proximal and medial/distal localities, we suggest that the pyroclastic-fall deposits were dispersed towards the N (e.g., EPPA-type tephras), the S/SE (both EPPA- and MPA-type tephras), and likely towards the E (LSPA-type tephra). Accordingly, detailed analyses on distal tephra occurrences from other recently identified sites are in progress, and expected to help with constructing more detailed tephra dispersal maps.

6. Summary and conclusions — late-stage volcanic and volcano geomorphic evolution

The results obtained in our multidisciplinary study cast new light on the explosive eruptions of Ciomadul volcano in terms of tephrostratigraphy, eruptive chronology, and moreover the evolution of successive venting. The volcanic history, comprising roughly the last ~50 ky, can be summarised as follows (Fig. 15).

1. Subsequent to a dome-building stage in the central dome complex (Fig. 15-1), the first explosive eruptions, grouped into EPPA (Early Phreatomagmatic and Plinian Activity), may have been initiated in a vent area at or around the present-day Mohoş crater (Fig. 15-2). A succession of phreatomagmatic events at ~51 ka, called Turia eruption(s), produced widespread tuffs with highly evolved rhyolitic glass composition and were distributed both to the N and S. The northern, prominent explosion crater (or caldera) rim of Ciomadul Mare may have also been shaped by these eruptions. Based on the preliminary interpretation of geoelectrical and sedimentological data, it appears that the lacustrine basin that formed within Mohoş crater has been archiving sediments and tephra layers since then, which provides a highly useful record of the proximal tephrostratigraphy.

2. As part of EPPA, the next important explosive phase, called BTS (for Băile Tuşnad), may indicate a shift of the vent area to a "Proto-St. Ana" crater. At ~≥43(-50) ka, plinian eruption(s) produced pumice fall and a pumiceous pyroclastic flow (Fig. 15-3) with EPPA-type glass compositions, with the pyroclastic material deposited (and/or slightly redeposited) on the steep W slope of Ciomadul. The BTS eruption may have been coeval with one of the final lava effusions (Piscul Pietros, ~43 ka) that produced a thick lava flow toward the SE.

3. A most likely quiescent period of ~10 ky followed. However, during this period, a non-explosive lava dome growth at or around the Proto-St. Ana crater, likely occurred (Fig. 15-4).

4. One of the most significant explosive eruptions at Ciomadul is grouped into the MPA (Middle Plinian Activity) stage. Its main phase, called TGS for one of the representative outcrops at the town of Târgu Secuiesc, terminated quiescent lava dome growth period at ~31.5 ka. During the eruption, the growing dome in the Proto-St. Ana crater was destroyed explosively, possibly together with a sustained vulcanian column/fountain

collapse, and produced a number of pumiceous block-and-ash flows toward the S and SE (Fig. 15-5). Several-m-thick deposits from this event can be found high in the stratigraphy (in gullies, valleys, and the Mohoş crater infill). Finally, although the chronology is not fully solved, we propose that a plinian column may have emerged from the open vent, generating pumice fallout toward distal areas (i.e. 0.6 m pumice-fall deposit 21 km from vent to the SE at TGS-1 locality; Fig. 15-6). Pumices of the MPA deposits display a characteristic, less evolved rhyolitic glass composition compared to the EPPA stage.

5. Ca. 2,000 years after the MPA eruptions, a newly discovered final stage termed LSPA (Latest St. Ana Phreatomagmatic Activity) terminated the volcanic activity of Ciomadul. This final phreatomagmatic eruption from the St. Ana vent is dated by radiocarbon at ~29.6 ka BP, and produced widespread, fine-grained tephra of more evolved rhyolitic glass composition toward the E–SE, blanketing the landscape (Fig. 15-7). We suggest that this final eruption may have been a violent, possibly phreatoplinian event, reflected by the present-day, enlarged (~1600 m wide) explosive crater of St. Ana.

Acknowledgements

D.K., E.M, R.G. and T.T. thank the Hungarian National Fund K115472, E.M and D.K. the Hungarian National Fund NF101362 for financial support. D.V. acknowledges the support by a grant of the Ministry of National Education of Romania CNCS–UEFISCDI, project number PN-II-ID-PCE-2012-4-0530. A.T.G. acknowledges financial support from the L'Oréal-UNESCO for Women in Science Fellowship. V.A.D. is grateful for financial support from the Sectorial Operational Programme for Human Resources 279 Development 2007-2013, co-financed by the European Social Fund, under the project 280 POSDRU/159/1.5/S/133391

– "Doctoral and postdoctoral excellence programs for training highly qualified 281 human resources for research in the fields of Life Sciences, Environment and Earth." Big thanks go to Richard Niederreiter and his UWITEC team who performed the coring of both craters (St. Ana in 2013 and Mohoş in 2014). Coring, respectively, was financially supported by the Hungarian National Fund NF101362 (St. Ana, 2013), and the German Science Foundation (DFG) as part of the CRC-806 "Our way to Europe" at Cologne University, Germany (Mohoş, 2014). We also thank the Cologne AMS ^{14}C lab of Janet Rethemeyer for the radiocarbon dating of the MOH-2 sediment core samples. Raman spectroscopy analysis by T. Váczi at the Research and Instrument Core Facility, Faculty of Science, Eötvös University, and lab help of MSc students Z. Cseri and M. Hencz, are appreciated. Comments on the assessment of radiometric dates by X. Quidelleur, constructive reviews of the manuscript by R. Escobar Wolf and an anonymous reviewer, as well as the editorial handling by J. Martí, are gratefully acknowledged.

Tables:

Table 1: Summary of volcanological and major element glass geochemical data of pyroclastic exposures around Ciomadul. For location, see text and Figs. 1 and 3. For description of units, see text. General references are given in the main text, only those specific to certain features appear here. Volcanic glass compositions, which are consistently rhyolitic, have been classified according to their main affinity (more silicic "EPPA"-, less silicic "MPA-" and intermediate silicic "LSPA-"type, see text); n.a. = not analyzed

Table 2: Comparison of (U-Th)/He, ^{14}C and luminescence age constraints of the past ~50 ky volcanic formations and embedding terrestrial and lacustrine deposits at Ciomadul volcano and within its twin-crater, St Ana and Mohoş

Figure captions:

Fig. 1: Topography of South Harghita Mts. and their vicinity on 30 m-resolution SRTM DEM with all medial-distal, and two proximal study sites (red circles) described in this paper. Inset map (upper left) shows the geographic position and main features of the volcanic range indicating the study area

Fig. 2: A: Tectonic setting of the study are within the southern part of East Carpathians (simplified after many authors, in particular Mațenco et al., 1997; Chalot-Prat and Gîrbacea, 2000); B: Volcanological sketch map of the Ciomadul volcano (lithology after Szakács and Seghedi, 1986; volcanic geomorphology after Karátson et al., 2013). Am = amphibole, bi = biotite, py = pyroxene, q = quartz, α = andesite, δ = dacite

Fig. 3: Oblique shaded and coloured DEM image of Ciomadul with proximal study sites (red), the St. Ana (SZA2013) and Mohoş (MOH-2) cores (blue), and the sections of the geoelectric survey of Mohoş crater (enlarged on top). Numbers on axes are UTM coordinates

Fig. 4: Proposed correlation scheme of the localities studied in this paper. Colour codes of units belonging to EPPA (black), MPA (orange) and LSPA (blue) stages are identical with those in Fig. 12.

Fig. 5. Main features of localities a) BIX-1 (Bixad/Sepsibükkszád village ~1 km E) and b) BIX-4 (Bixad village ~2.5 km NE). For BIX-1.2, granulometry and clast size density are shown

Fig. 6. Main features of locality BOL-1 (W slopes of M. Balondoș/Bolondos hill). Insets show BOL-1.3 and 1.4 identified at another part of the outcrop. For BOL-1.2, granulometry is also displayed

Fig. 7. Main features of locality MOH-PR-1 (Mohoş outlet gorge of P. Rosu/Veres-patak) with granulometry for MOH-1.3/1.4 and OSL age constraints. Stratigraphic log after Karátson (2007), slightly modified.

Fig. 8. A) Main features of locality TGS-1 (abandoned quarry ~0.5 km N of Târgu Secuiesc/Kézdivásárhely), with granulometry for TGS-1-1; B): OSL sampling site and results as shown in Harangi et al. (2015); C) OSL sampling site of this study with obtained results

Fig. 9. Main features of localities A) TUR-2 (abandoned roadside quarry ~0.5 km W of Turia/Torja village) with granulometry for TUR-2.2, and B) SNM-1 (abandoned pit quarry ~0.5 km N of Sânmartin/Csíkszentmárton village) with granulometry for SNM-1.1 and -1.2, in both cases with OSL age constraints

Fig. 10: Results of grain size analysis of the studied Ciomadul pyroclastic units plotted in the sorting vs median diameter (σφ/Mdφ) diagram. Grainsize distribution of individual units of pyroclastic-fall deposits is shown in the upper left, that of pyroclastic-flow deposits in the upper right diagram, respectively. In comparison with the Ciomadul samples, dots of block-and-ash flows of the 1886 Kaharoa eruptive episode of Tarawera domes (Hanenkamp, 2011) and those of the 2010 Merapi eruption (Charbonnier et al., 2013) are also plotted.

Fig. 11: Componentry of selected pyroclastic deposits. Left: lithic clasts and xenoliths from the pumiceous block-and-ash flow deposits from the proposed first phase of TGS eruption (MPA stage; upper left) and the pumiceous pyroclastic-flow deposit of the BTS eruption (EPPA stage; lower left); right: pumiceous clasts of pyroclastic-flow (top) and -fall deposits (bottom) from the TGS eruption

Fig. 12: (A) Bi-variate plots of major element glass compositions of medial-distal (A) and proximal (B) tephra units from Ciomadul discriminating three main eruption types: "EPPA-type" (black symbols), "MPA-type" (orange symbolst) and "LSPA-type" (blue symbols). The coloured envelopes represent all samples that have been correlated with the respective type of eruptive stage based on stratigraphical field evidence and granulometric data.

Fig. 13: Transmitted light (upper row) and BSE (secondary electron) images (lower row) of juvenile clasts (volcanic glass shards, micropumices) and phenocrysts from tephra layers of EPPA-type (left column, unit TUR-2.1), MPA-type (middle column, unit TGS-1.1) and LSPA-type (right column, unit RO-1/2/3) eruptions. Note the high abundances of feldspar microcryst inclusions (fs; lighter needle-shape minerals) in all EPPA- and LSPA-type and some MPA-type pumices (SE images)

Fig. 14: Photo compilation of the ~13 to 15.7 m section of the Mohoş MOH-2 core with obtained radiocarbon ages

Fig. 15: Proposed summary of the last ~50 ky of Ciomadul's eruptive chronology as represented by successive stages of the volcano-geomorphic evolution

Supplementary files:

Supplement 1: Density measurement results of the BIX-1.2 pumiceous clasts
Supplement 2: EPMA raw and normalized (volatile-free) chemical data of Ciomadul tephras and secondary glass standards
Supplement 3: Pollen extraction procedure for AMS ^{14}C dating
Supplement 4: Optically stimulated luminescence (OSL) methodology

Supplementary figures:

Suppl. fig. 1: Main features and stratigraphic sketch of locality BTS-1 (Băile Tuşnad/ Tusnádfürdő) locality, with granulometry for BTS-1.3 'C'. Inset stratigraphic log after Moriya et al. (1995)

Suppl. fig. 2. Main features of localities a) RPSA-1 (Románpuszta roadside quarry toward St. Ana) with granulometry for RSPA-1.2, and b) BIX-2 (Bixad village ~1.5 km S); arrow points to a prismatically jointed block

Suppl. fig. 3. Main features of localities a) MOH-VM-1 (trail cut ~0.5 km under the hill of Vf. Mohoş/Mohos-tető], with granulometry for MOH-VM-1.3, and b) SFA (St. Ana crater inner slopes at Belvedere outlook point)

References

Adamiec G, Aitken M., 1998. Dose-rate conversion factors: update. Ancient TL 16 (2), 37–50.

Anechitei-Deacu V., Timar-Gabor A., Fitzsimmons K.E., Veres D., Hambach U., 2014. Multi-method luminescence investigations on quartz grains of different sizes extracted from a loess section in southeast Romania interbedding the Campanian Ignimbrite ash layer. Geochronometria 41 (1), 1–14.

Bányai, J., 1917. Kézdivásárhely vidéke Háromszék vármegyében (The land of Kézdivásárhely in Háromszék county; in Hungarian). Földtani Közlöny (Bull. Hung. Geol. Soc.), XLVII, 1–20.

Bányai, J., 1964. The eruptive age of Lake Szent Anna twin craters (A Szent Anna-tavi ikerkráter erupciójának kora; in Hungarian). Földrajzi Értesítő (Hung. Geogr. Bull.), XIII (1), 57–66.

Bulla, B., 1948. A két Csiki-medence és az Olt-völgy kialakulásáról (On the formation of the two Ciuc Basins and Olt valley; in Hungarian). Földrajzi Közlemények (Bull. Hung. Geogr. Soc.) LXXVI, 134-156.

Buylaert, J.P., Thiel, C., Murray, A.S., Vandenberghe, D.A.G., Yi, S., Lu, H., 2011. IRSL and post-IR IRSL residual doses recorded in modern dust samples from the Chinese Loess Plateau. Geochronometria 38, 432-440.

Casta, L., 1980. Les formation quaternaires de la depression de Brasov (Roumaine). PhD Thesis, Université d'Aix Marseille II, 256 p.

Chalot-Prat, F., Gîrbacea, R., 2000: Partial delamination of continental mantle lithosphere, uplift-related crust-mantle decoupling, volcanism and basin formation: a new model for the Pliocene-Quaternary evolution of the sourthern East-Carpathians, Romania. Tectonophysics 327, 83-107.

Charbonnier, S. J., Gertisser, R., 2008. Field observations and surface characteristics of pristine block-and-ash flow deposits from the 2006 eruption of Merapi Volcano, Java, Indonesia. J. Volcanol. Geotherm. Res. 177 (4), 971–982.

Charbonnier, S.J., Germa, A., Connor, C.B., Gertisser, R., Komorowski, J.-C., Preece, K., Lavigne, F., Dixon, T., Connor, L., 2013. Evaluation of the impact of the 2010 pyroclastic density currents at Merapi volcano from high-resolution satellite imagery, field investigation and numerical simulations. J. Volcanol. Geotherm. Res. 261, 295–315.

Cholnoky, J., 1922. Néhány vonás az Erdélyi-medence földrajzi képéhez. III. Hargita (Contributions to the geography of Transylvanian Basin. III. Harghita Mts. – in Hungarian). Földrajzi Közlemények (Bull. Hung. Geogr. Soc.), Budapest, 50 (2), 107–122.

Constantin D., Timar-Gabor A., Veres D., Begy R., Cosma C., 2012. SAR-OSL dating of different grain-sized quartz extracted from a sedimentary section in southern Romania interbedding the Campanian Ignimbrite/Y5 ash layer. Quaternary Geochronology 10, 81–86.

Druitt, T. H. et al., 2002. Episodes of cyclic Vulcanian explosive activity with fountain collapse at Soufrière Hills Volcano, Montserrat. In: Druitt, T.H., Kokelaar, R. (eds.), The Eruption of Soufrière Hills Volcano, Montserrat from 1995 to 1999. Geol. Soc. Mem. 21, 281–306.

Eshel, G., Levy, J., Mingelgrin, U.,Singer, M.J., 2004. Critical Evaluation of the Use of Laser Diffraction for Particle-Size Distribution Analysis. Soil Science Society America Journal 68, 736–743

Fichtel, J.E. von. 1780. Beytrag zur Mineralgeschichte von Siebenbürgen. Zweyter Theil welcher die Geschichte des Steinsalzes enthält. Raspische Buchhandlung, Nürnberg, 134 p.

Fielitz, W., Seghedi, I., 2005. Late Miocene-Quaternary volcanism, tectonics and drainage system evolution on the East Carpathians, Romania. In: Cloetingh, S. et al. (eds.): Special volume fourth Stephan Müller conference of the EGU on geodynamic and tectonic evolution of the Carpathian Arc and its foreland. Tectonophysics 410, 111–136.

Fitzsimmons, K.E., Hambach U., Veres D., Iovita R., 2013. The Campanian Ignimbrite eruption: new data on volcanic ash dispersal and its potential impact on human evolution. PlosOne 8 (6), article e65839.

Frechen, M., Schweitzer, U., Zander, A., 1996. Improvements in sample preparation for the fine grain technique. Ancient TL 14 (2), 15–17.

Freundt, A., Wilson, C.J.N., Carey, S.N., 1999. Ignimbrites and Block-And-Ash Flow Deposits. In: Sigurdsson, H. et al. (eds.), Encyclopedia of Volcanoes. Academic Press, pp. 581–599.

Hanenkamp, E., 2011. Decoupling processes in block-and-ash flows: field evidence and analogue modelling. PhD Thesis, University of Canterbury, 254 p.

Harangi, Sz., Molnár, M., Vinkler, A. P., Kiss, B., Jull, A. J. T., Leonard, A. E., 2010. Radiocarbon dating of the last volcanic eruptions of Ciomadul volcano, Southeast Carpathians, eastern-central Europe. Radiocarbon, 52 (2-3), 1498–1507.

Harangi, Sz., Lukács, R., Schmitt, A.K., Dunkl, I., Molnár, K., Kiss, B., Seghedi, I., Novothny, Á., Molnár, B., 2015. Constraints on the timing of Quaternary volcanism and duration of magma residence at Ciomadul volcano, east–central Europe, from combined U–Th/He and U–Th zircon geochronology. J. Volcanol. Geotherm. Res. 301, 66–80.

Hauer, F.R. von, Stache, G., 1863. Geologie Siebenbürgens. Verein für Siebenbürgische Landeskunde, W. Braumüller, Wien, 636 p.

Horiba, 2008. AN157 applications note. Refractive index selection for powder mixtures. Horiba Instruments Inc., 1 p.

Horiba Partica LA-950 V2, 2013. http://www.horiba.com/investor-relations/ir-library/horiba-report/

Hunt, J. B., Hill, P.G., 1996. An inter-laboratory comparison of the electron probe microanalysis of glass geochemistry. Quaternary International 34-36, 229–241.

Kuehn, S.C., Froese, D.G., Shane, P.A.R., 2011. The INTAV intercomparison of electron-beam microanalysis of glass by tephrochronology laboratories, results and recommendations. Quaternary International 246, 19–47.

Jánosi, Cs. 1983. Prospecțiuni pentru piatră ponce in perimetrul Tușnad–Bixad (Județele Harghita, Covasna), Scale 1:5000. Unpublished geological report, I.P.E.G., Miercurea Ciuc, Romania.

Karátson, D., 2007. A Börzsönytől a Hargitáig – vulkanológia, felszínfejlődés, ősföldrajz (From Börzsöny to Harghita Mts. – volcanology, surface evolution, paleogeography; in Hungarian). Typotex Kiadó, Budapest, 463 p.

Karátson, D., Timár, G., 2005. Comparative volumetric calculations of two segments of the Neogene/Quaternary volcanic chain using SRTM elevation data: implications for erosion and magma output rates. Z. Geomorphol. Suppl. 140, 19–35.

Karátson, D., Telbisz, T., Harangi, S., Magyari, E., Dunkl, I., Kiss, B., Jánosi, C., Veres, D., Braun, M., Fodor, E., Biró, T., Kósik, S., von Eynatten, H., Lin, D., 2013. Morphometrical and geochronological constraints on the youngest eruptive activity in East-Central Europe at the Ciomadul (Csomád) lava dome complex, East Carpathians. J. Volcanol. Geotherm. Res. 255, 43–56.

Kiss, B., Harangi, S., Ntaflos, T.,Mason, P.R.D., Pál-Molnár, E., 2014. Amphibole perspective to unravel pre-eruptive processes and conditions in volcanic plumbing systems

beneath intermediate arc volcanoes: a case study from Ciomadul volcano (SE Carpathians). Contrib. Mineral. Petrol. 167, 986.

Komorowski, J.-C., Jenkins, S., Baxter, P., Picquout, A., Lavigne, F., Charbonnier, S.J., Gertisser, R., Preece, K., Cholik, N., Budi-Santoso, A., Surono, 2013. Paroxysmal dome explosion during the Merapi 2010 eruption: Processes and facies relationships of associated high-energy pyroclastic density currents. J. Volcanol. Geotherm. Res., 261, 260–294.

Kristó, A., 1957. A Csiki-medencék geomorfológiai problémái (Geomorphological problems of the Ciuc Basin; in Hungarian). A Csiki Múzeum Közleményei (Annals of the Csiki Museum), Miercurea Ciuc, 23–50.

Lang, A., Lindauer, S., Kuhn, R., Wagner, G.A., 1996. Procedures used for optically and infrared stimulated luminescence dating of sediments in Heidelberg. Ancient TL 14 (3), 7–11.

Loke, M.H., Barker, R.D., 1996. Practical techniques for 3D resistivity surveys and data inversion. Geophysical Prospecting 44 (3), 499–523.

Macías, J.L., Capra, L., Arce, J.L., Espíndola, J.M., García-Palomo, A., Sheridan, M.F., 2008. Hazard map of El Chichón volcano, Chiapas, México: Constraints posed by eruptive history and computer simulations. J. Volcanol. Geotherm. Res. 175, 444–458

Magyari, E.K., Buczkó, K., Jakab, G., Braun, M., Szántó, Zs, Molnár, M., Pál, Z., Karáatson, D., 2006. Holocene palaeohydrology and environmental history in the South Harghita Mountains, Romania. Földtani Közlöny 136, 249–284.

Magyari, E.K., Buczkó, K., Jakab, G., Braun, M., Pál, Z., Karátson, D., 2009. Palaeolimnology of the last crater lake in the Eastern Carpathian Mountains – a multiproxy study of Holocene hydrological changes. Hydrobiologia 631, 29–63.

Magyari, E. K., Veres, D., Wennrich, V., Wagner, B., Braun, M., Jakab, G., Karátson, D., Pál, Z., Ferenczy, Gy, St-Onge, G., Rethemeyer, J., Francois, J.-P., von Reumont, F., Schäbitz, F., 2014. Vegetation and environmental responses to climate forcing during the Last Glacial Maximum and deglaciation in the East Carpathians: attenuated response to maximum cooling and increased biomass burning. Quaternary Science Reviews 106, 278–298.

Maeno, F., Nakada, S., Yoshimoto, M., Shimano, T., Hokanishi, N., Akhmad, Z., Iguchui, M., 2014. Plinian eruption preceded by disruption of lava dome at Kelud volcano, Indonesia, in 2014. Japan Geoscience Union Meeting, SVC46-08.

Mason, P. R. D., Seghedi, I., Szakács, A., Downes, H., 1998. Magmatic constraints on geodynamic models of subduction in the Eastern Carpathians, Romania. Tectonophysics 297, 157–176.

Mațenco, L., Zoetemeijer, R., Cloetingh, S., Dinu, C., 1997. Lateral variations in mechanical properties of the Romanian external Carpathians - Inferences of flexure and gravity modelling. Tectonophysics, 282 (1-4), 147-166.

Michailova, N., Glevasovskaja, A., Sykora, V., Nestianu, I., Romanescu, D. 1983. New paleomagnetic data for the Călimani, Gurghiu and Harghita volcanic Mountains in the Romanian Carpathians. An. Inst. Geol. Geofiz. 63, 101–111.

Molnár, M., Janovics, R., Major, I., 2013. Status Report of the New AMS ^{14}C Sample Preparation Lab of the Hertelendi Laboratory of Environmental Studies (Debrecen, Hungary). Radiocarbon 55, 665–676. doi:10.2458/azu_js_rc.55.16394

Moriya, I., Okuno, M., Nakamura, E., Szakács, A., Seghedi, I., 1995. Last eruption and its ^{14}C age of Ciomadul volcano, Romania. Summaries of Researches using AMS, Nagoya University 6, 82–91.

Moriya, I., Okuno, M., Nakamura, T., Ono, K., Szakács, A., Seghedi, I. 1996, Radiocarbon ages of charcoal fragments from the pumice flow deposit of the last eruption of Ciomadul volcano, Romania. Summaries of Researches using AMS, Nagoya University 7, 255–257.

Murray, A.S., Wintle, A.G., 2000. Luminescence dating of quartz using an improved single-aliquot regenerative-dose protocol. Radiation Measurements 32, 57–73.

Murray, A.S., Wintle, A.G., 2003. The single aliquot regenerative dose protocol: potential for improvements in reliability. Radiation Measurements 37, 377–381.

Panait, A.M., Tanțău, I., 2012: Late Holocene vegetation history in Harghita Mountains (Romania). Georeview – Scientific Annals of Stefan cel Mare University Suceava, Geography Series 21, 93–99.

Pécskay, Z., Szakács, A., Seghedi, I., Karátson, D., 1992. Contributions to the geochronology of Mt. Cucu volcano and the South Harghita (East Carpathians, Romania). Földtani Közlöny, 122 (2-4), 265–286.

Pécskay, Z., Lexa, J., Szakács, A., Balogh, K., Seghedi, I., Konecny, V., Kovács, M., Márton, E., Kaliciak, M., Széky-Fux, V., Póka, T., Gyarmati, P., Edelstein, O., Rosu, E., Žec, B., 1995. Space and time distribution of Neogene-Quaternary volcanism in the Carpatho-Pannonian Region. Acta Vulcanologica 7 (2), 15–28.

Pécskay, Z., Lexa, J., Szakács, A., Seghedi, I., Balogh, K., Konečný, V., Zelenka, T., Kovacs, M., Póka, T., Fülöp, A., Márton, E., Panaiotu, C., Cvetković, V., 2006. Geochronology of Neogene-Quaternary magmatism in the Carpathian arc and intra-Carpathian area: a review. Geologica Carpathica 57, 511–530.

Peltz, S., 1971. Contribuții la cunoaşterea formațiunii vulcanogen-sedimentare pleistocene din sudul munților Harghita şi nord-estul bazinului Baraolt (Contibution to the knowledge on the Pleistocene volcanogenic sedimentary formations from the S of Mt. Harghita to the NE of Baraolt basin – in Romanian). D. S. Inst. Geol. Geofiz., LVII (5), 173–189.

Popa, M., Radulian, M., Szakács, A., Seghedi, I., Zaharia, B., 2012. New seismic and tomography data in the southern part of the Harghita mountains (Romania, Southeastern Carpathians): connection with recent volcanic activity. Pure Appl. Geophys. 169, 1557–1573.

Preparation Lab of the Hertelendi Laboratory of Environmental Studies (Debrecen, Hungary). Radiocarbon 55, 665–676. doi:10.2458/azu_js_rc.55.16394

Rădulescu, D.P., 1973. Le volcanisme explosive dans la partie de sud-est de Monts Harghita. Ann. Univ. Bucureşti 22, 7-16.

Reimer, P.J., Bard, E., Bayliss, A., Beck, J.W., Blackwell, P.G., Bronk, Ramsey C., Buck, C.E., Cheng, H., Edwards, R.L., Friedrich, M., Grootes, P.M., Guilderson, T.P., Haflidason, H., Hajdas, I., Hatté, C., Heaton, T.J., Hogg, A.G., Hughen, K.A., Kaiser, K.F., Kromer, B., Manning, S.W., Niu, M., Reimer, R.W., Richards, D.A., Scott, E.M., Southon, J.R., Turney, C.S.M., van der Plicht, J., 2013. IntCal13 and MARINE13 radiocarbon age calibration curves 0-50000 years calBP. Radiocarbon 55(4), 1869–1887.

Rethemeyer, J., Fülöp, R.-H., Höfle, S., Wacker, L., Heinze, S., Hajdas, I., Patt, U., König, S., Stapper, B., Dewald, A., 2013. Status report on sample preparation facilities for ^{14}C analysis at the new Cologne AMS center. Nuclear Instruments and Methods in Physics Research Section B, Beam Interactions with Materials and Atoms 294, 168–172.

Rowel, D.L. 1994. Soil science: methods and applications. Prentice Hall, London. 350 p.

Schreiber, W., 1972. Incadrarea geografica şi geneza Masivului Ciomadu (Geographic division and genesis of the Ciomadu Massif; in Romanian). Studia Universitatis Babeş-Bolyai, ser. Geographia, Cluj 1, 47–55.

Seghedi, I., Downes, H., Szakács, A., Mason, P. R. D., Thirlwall, M. F., Rosu, E., Pécskay, Z., Márton, E., Panaiotu, C. 2004. Neogene/Quaternary magmatism and geodynamics in the Carpathian-Pannonian region: a synthesis. Lithos 72, 117-146.
Seghedi, I., Downes, H., Harangi, S., Mason, P.R.D. and Pécskay, Z., 2005. Geochemical response of magmas to Neogene-Quaternary continental collision in the Carpathian-Pannonian region: A review. Tectonophysics 410 (1-4), 485–499.

Szakács, A., Jánosi, Cs., 1989. Volcanic bombs and blocks in the Harghita Mts. D. S. Inst. Geol. Geofiz. 74 (1), 181–189.

Szakács, A., Seghedi, I., 1986. Chemical diagnosis of the volcanics from the southernmost part of the Harghita Mountains—proposal for a new nomenclature. Rev. Roum. Geol. Geophys. Geogr., ser. Geologie 30, 41–48.

Szakács, A., Seghedi, I., 1989. Base surge deposits in the Ciomadul Massif (South Harghita Mts.). D. S. Inst. Geol. Geofiz. 74/1, 175–180.

Szakács, A., Seghedi I., 1990. Quaternary dacitic volcanism in the Ciomadul massif (South Harghita Mts, East Carpathians, Romania). IAVCEI International Volcanological Congress, 3-8 Sept., Abstract Volume, Mainz.

Szakács, A., Seghedi, I., 1995. The Călimani–Gurghiu–Harghita volcanic chain, East Carpathians, Romania: volcanological features. Acta Vulcanologica 7, 145–155.

Szakács, A., Seghedi, I., 1996. Neogene/Quaternary volcanism in Romania. In: Seghedi I. (ed.), Excursion guide A. The 90th anniversary conference of the Geological Institute of Romania, June 12-19, 1996. An. Inst. Geol. Geofiz. 69, suppl. 2, 33–42.

Szakács, A., Seghedi, I., Pécskay, Z., 1993. Pecularities of South Harghita Mts. as the terminal segment of the Carpathian Neogene to Quaternary volcanic chain. Rev. Roum. Geol. Geophys. Geogr., ser. Geologie 37, 21–36.

Szakács, A., Seghedi, I., Pécskay, Z., 2002. The most recent volcanism in the Carpathian-pannonian Region. Is there any volcanic hazard? Geologica Carpathica Special Issue, Proceedings of the XVIIth Congress of Carpatho-Balkan Geological Association, 53, pp. 193–194.

Szakács, A., Seghedi, I., Pécskay, Z.,Mirea, V., 2015. Eruptive history of a low-frequency and low-output rate Pleistocene volcano, Ciomadul, South Harghita Mts., Romania. Bull. Volcanol. 77, 12, DOI:10.1007/s00445-014-0894-7.

Tanțău, I., Reille, M., de Beaulieu, J.L., Farcas, S., Goslar, T., Paterne, M., 2003. Vegetation history in the eastern Romanian Carpathians: pollen analysis of two sequences from the Mohoş crater. Veg. Hist. Archaeobot. 12, 113–125.

Teulade, A., 1989. Téphrologie des formations cendro-ponceuses en mileux lacustres Quaternaires. Méthode et applications au Massif Central francais (Velay) et aux Carpathes orientales roumaines (dépression de Brasov). PhD. thesis. Université d'Aix-Marseiulle II., 298 p.

Varga, Gy., Újvári, G., Kovács, J., Szalai, Z., 2015. Effects of particle optical properties on grain size measurements of aeolian dust deposits. Geophys. Res. Abstracts 17 Paper, EGU2015-9848-1.

Vaselli, O., Minissale, A., Tassi, F., Magro, G., Seghedi, I., Ioane, D., Szakács, A., 2002. A geochemical traverse across the Eastern Carpathians (Romania): constraints on the origin and evolution of the mineral water and gas discharges. Chemical Geology, 182, 637–654.

Veres D., Lane S.C., Timar-Gabor A., Hambach H., Constantin D., Szakacs A., Fülling A., Onac B.P., 2013. The Campanian Ignimbrite/Y5 tephra layer – a regional stratigraphic marker for Isotope Stage 3 deposits in the Lower Danube region, Romania. Quaternary International 293, 22–33.

Vinkler, A. P., Harangi, Sz., Ntaflos, T., Szakács, A., 2007. A Csomád vulkán (Keleti-Kárpátok) horzsaköveinek kőzettani és geokémiai vizsgálata – petrogenetikai következtetések (Petrology and geochemistry of the pumices from the Ciomadul volcano [Eastern Carpathians] – implications for the petrogenetic processes). Földtani Közlöny 137, 103–128.

Walker, G.P.L., 1971. Grain-size characteristics of pyroclastic deposits. J. Geology 79, 696–714.

Wintle A.G., Murray A.S., 2006. A review of quartz optically stimulated luminescence characteristics and their relevance in single-aliquot regeneration dating protocols. Radiation Measurements 41, 369–391.

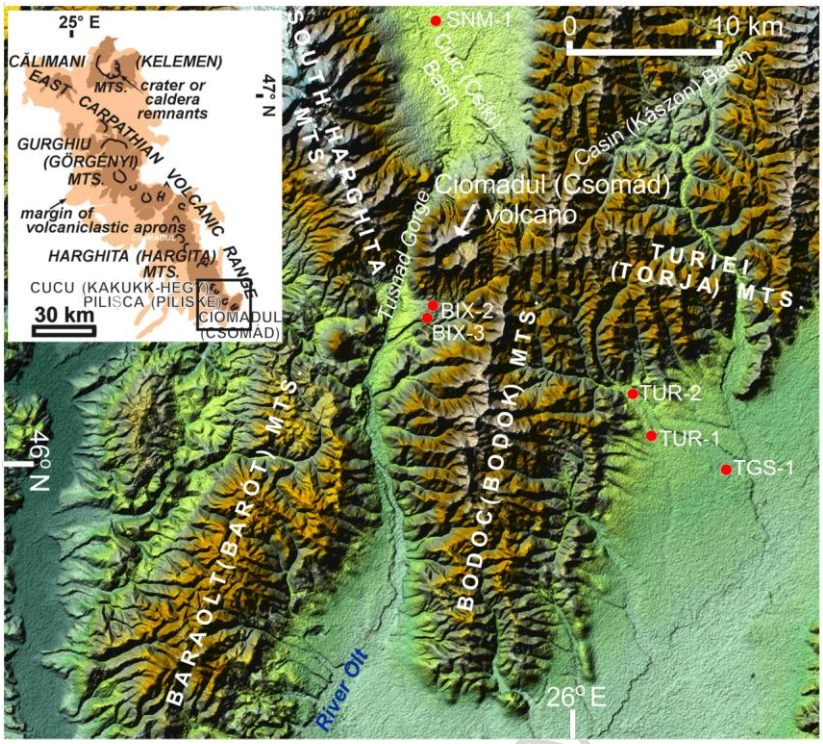

Figure 1

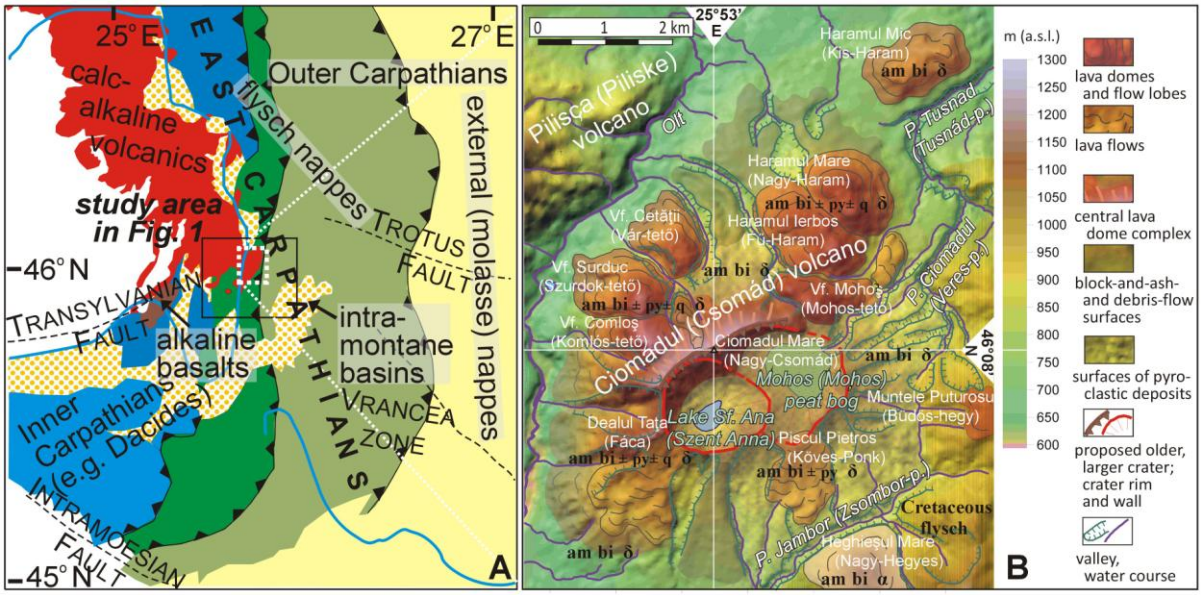

Figure 2

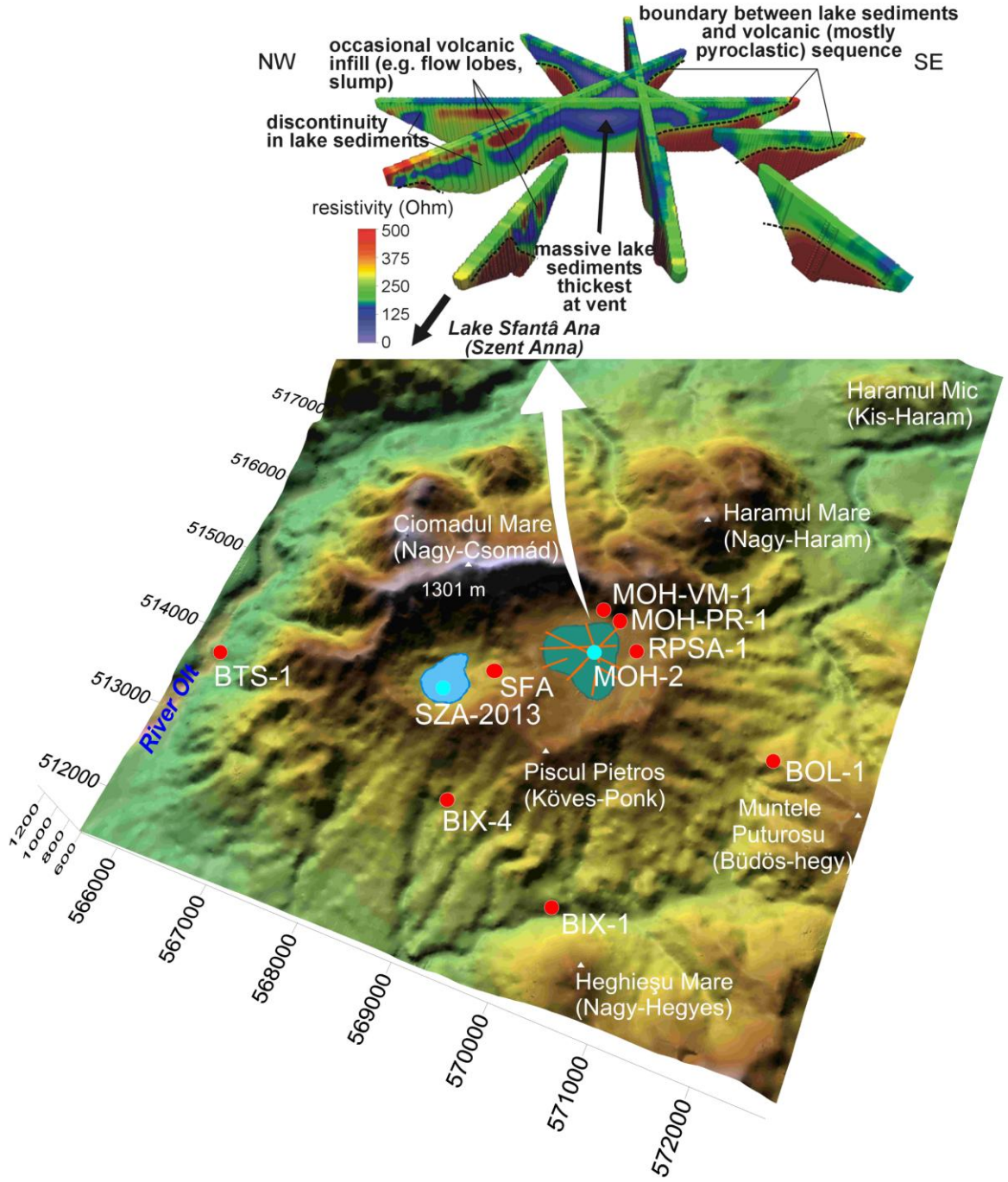

Figure 3

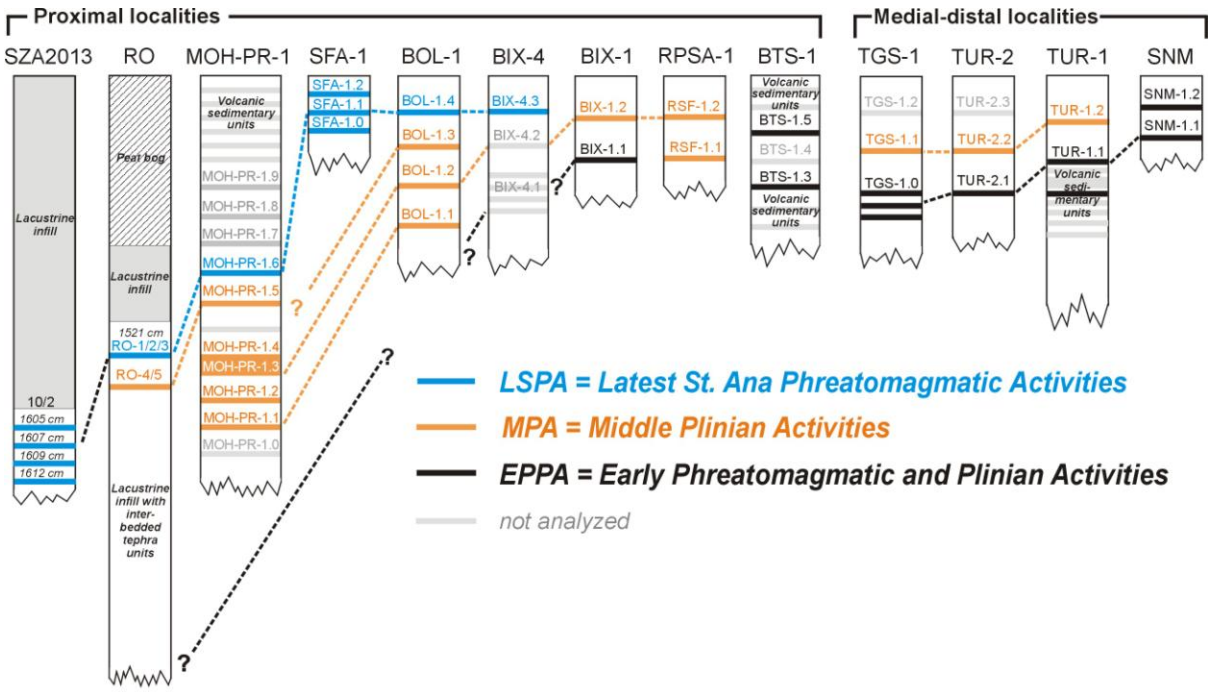

Figure 4

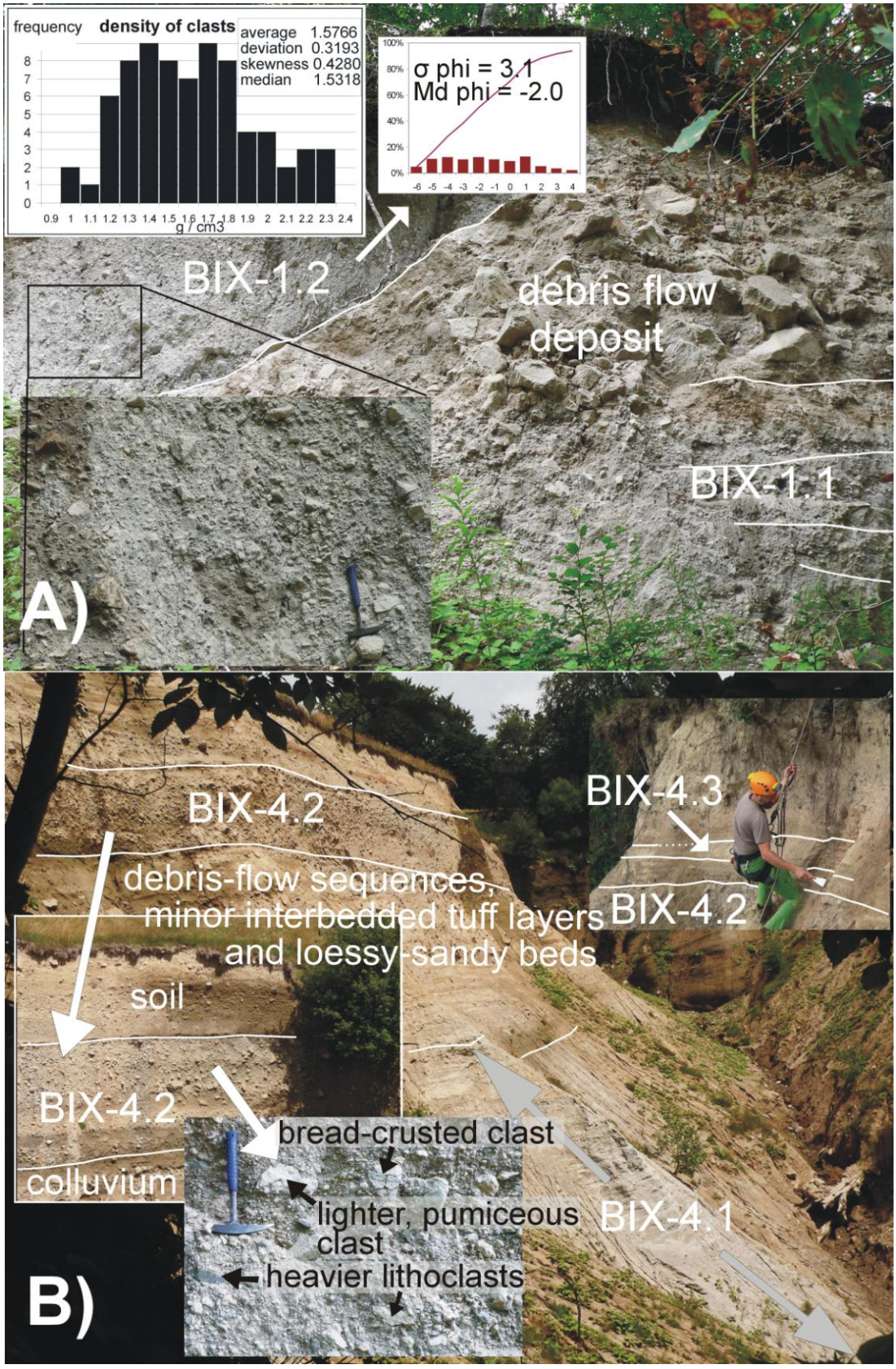
frequency
density of clasts
average 1.5766
deviation 0.3193
skewness 0.4280
median 1.5318
g / cm3
σ phi = 3.1
Md phi = -2.0
BIX-1.2
debris flow deposit
BIX-1.1
A)
BIX-4.2
BIX-4.3
debris-flow sequences, minor interbedded tuff layers and loessy-sandy beds
BIX-4.2
soil
BIX-4.2
colluvium
bread-crusted clast
lighter, pumiceous clast
heavier lithoclasts
BIX-4.1
B)

Figure 5

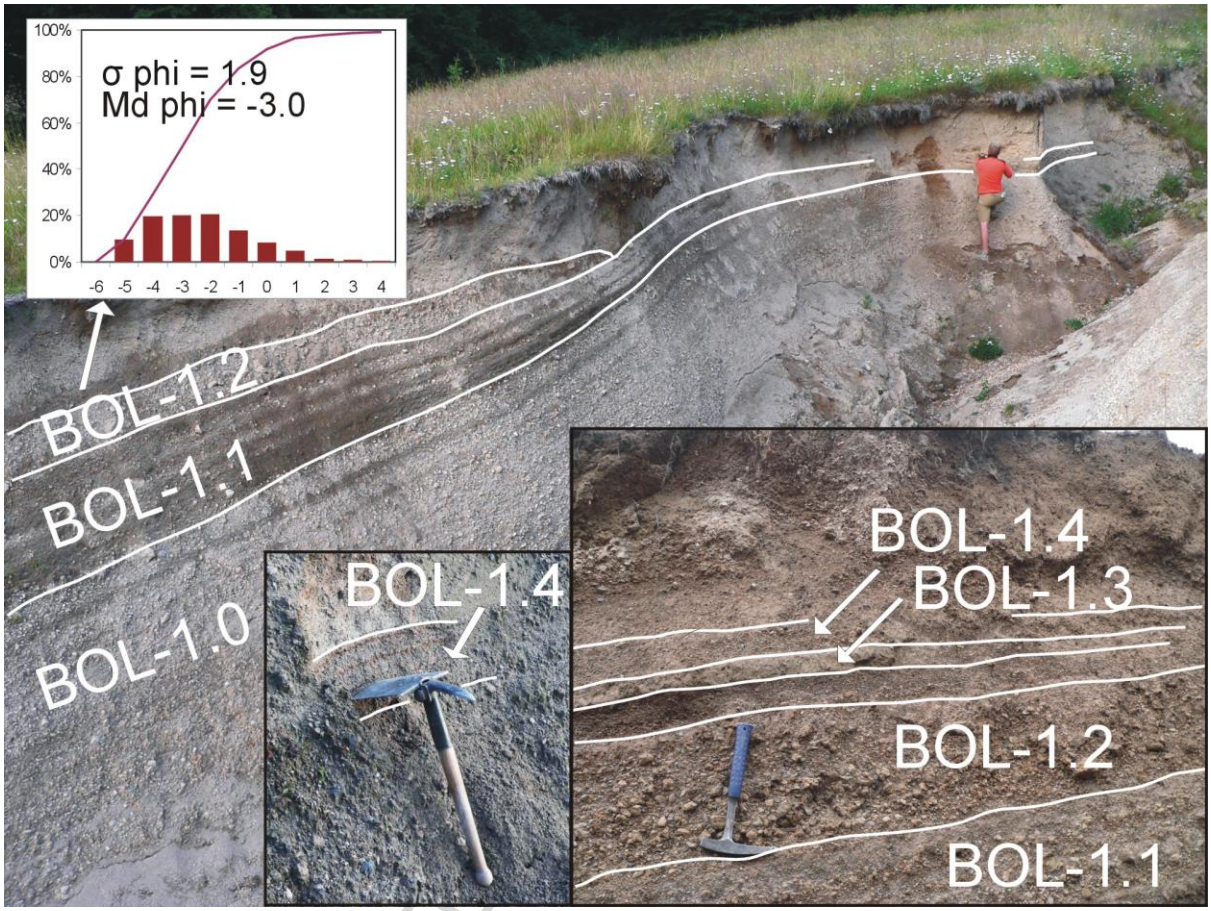

Figure 6

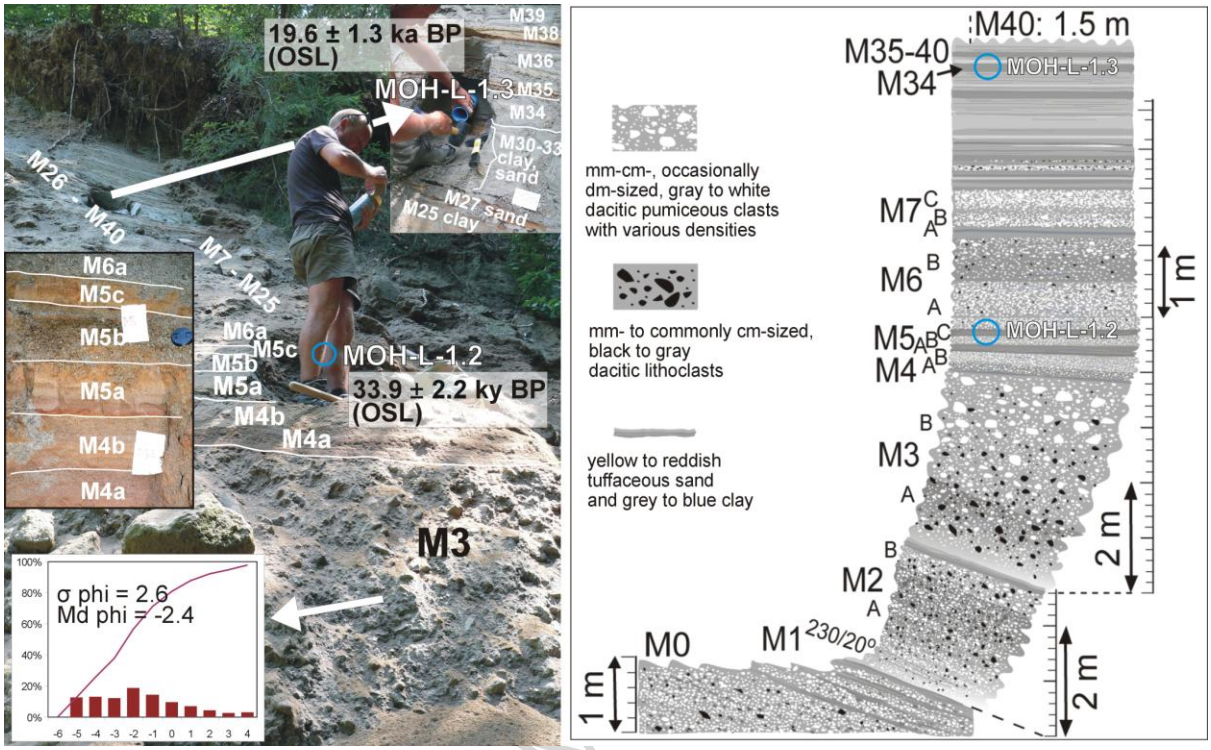

Figure 7

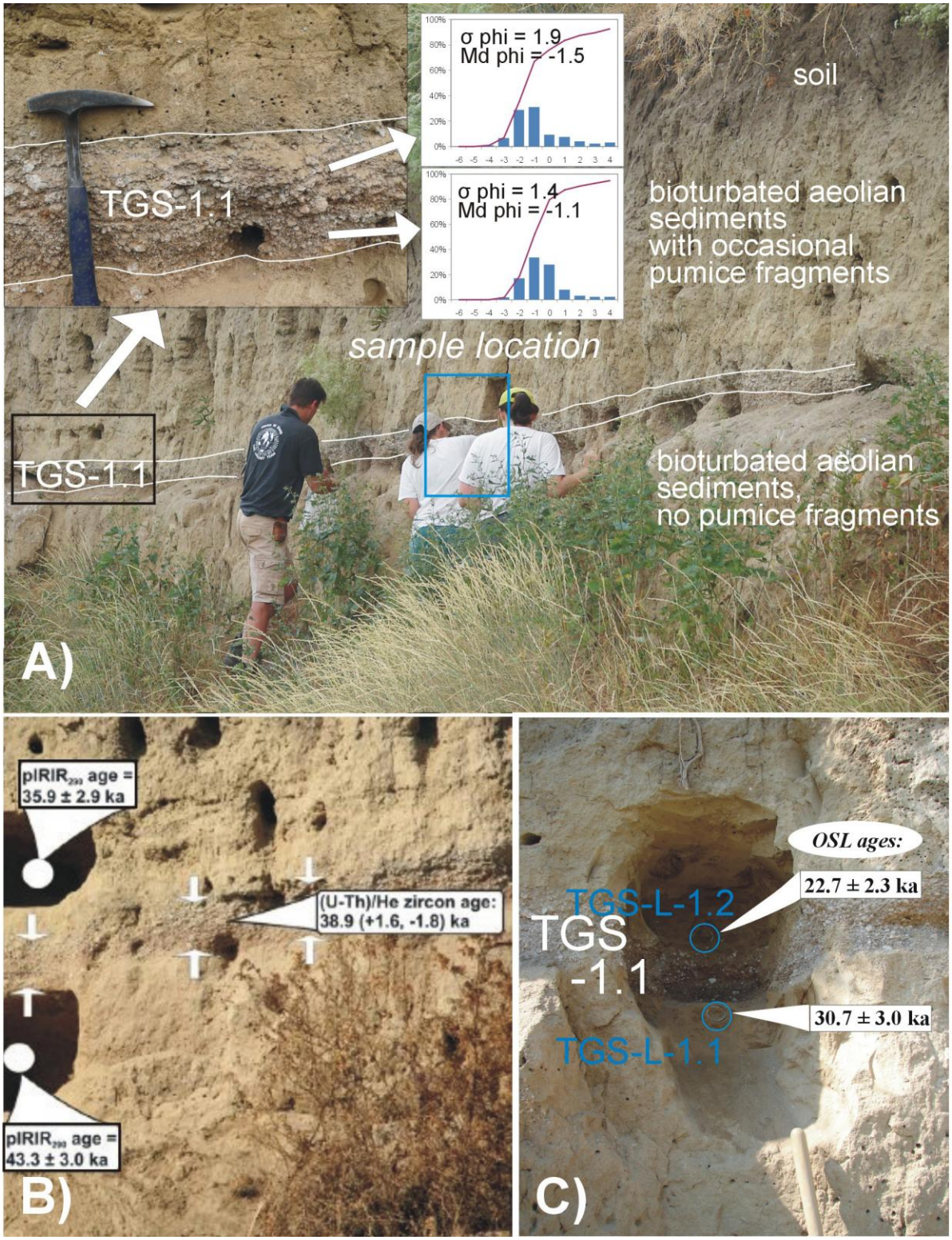

Figure 8

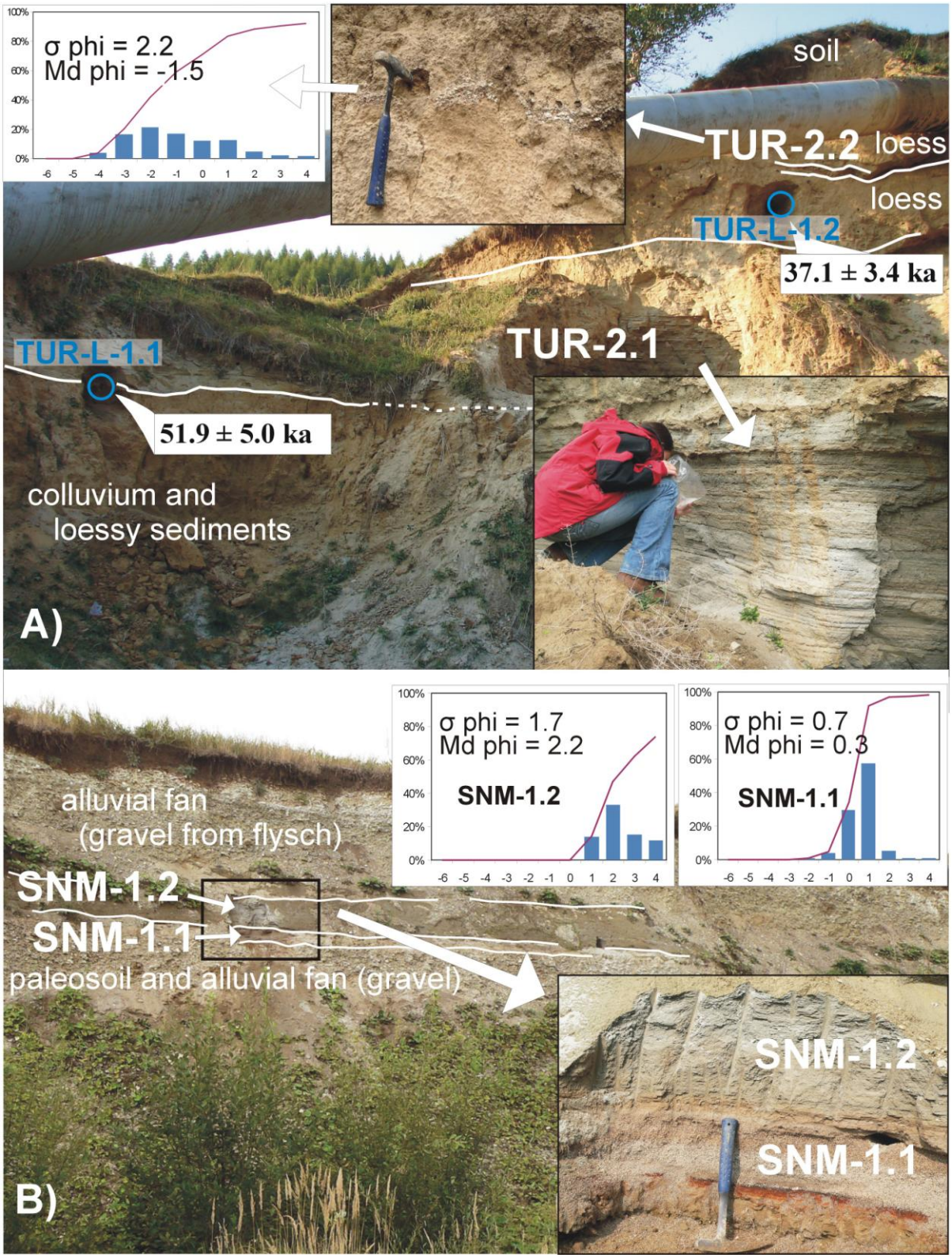

Figure 9

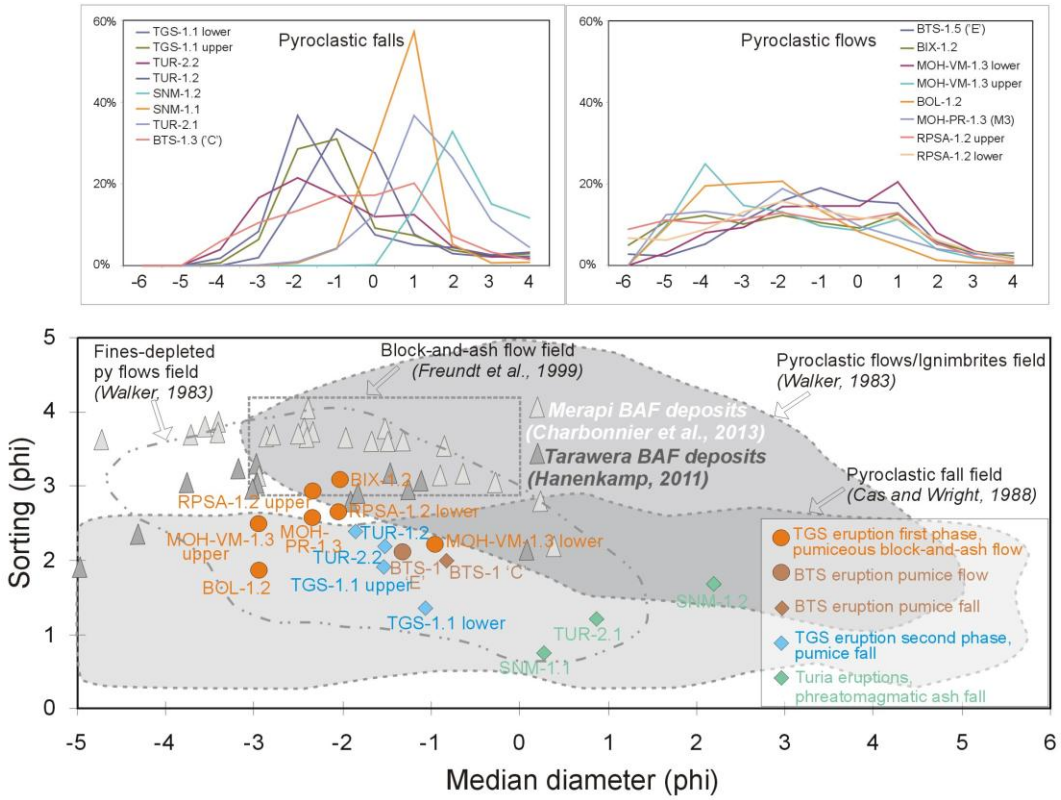

Figure 10

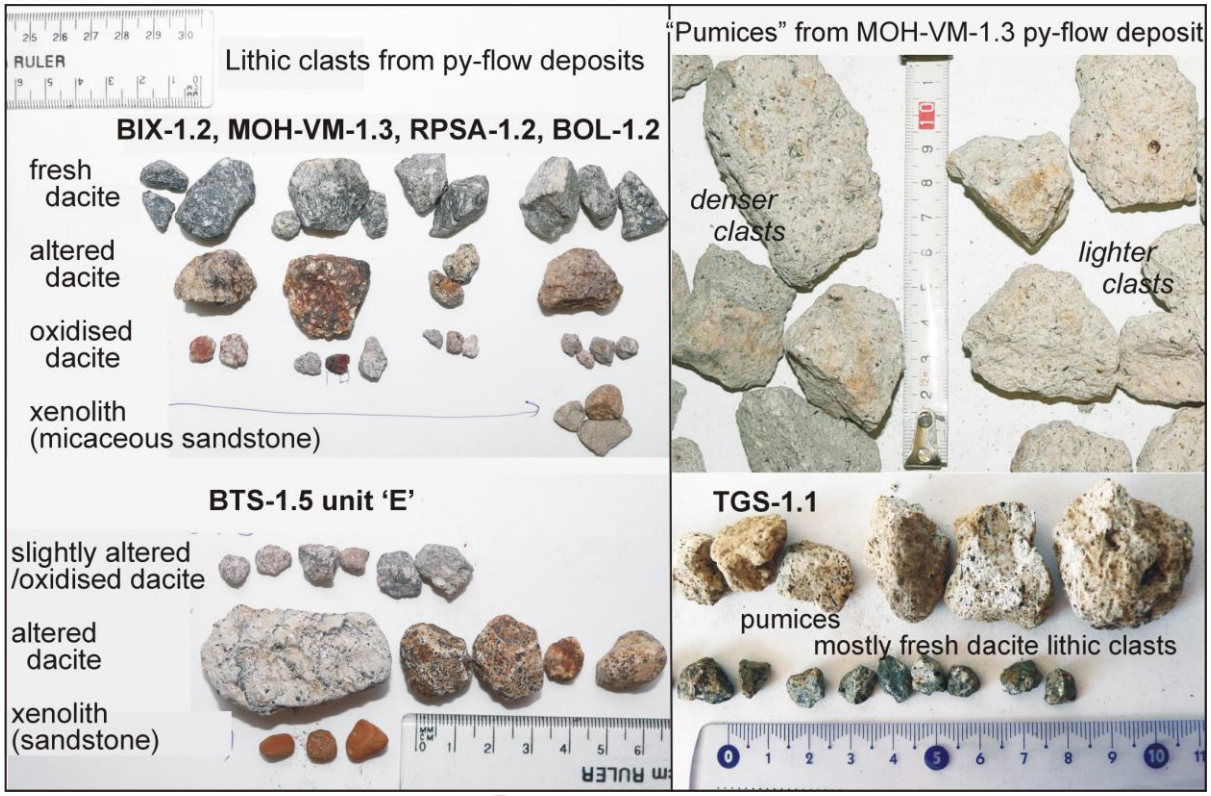

Figure 11

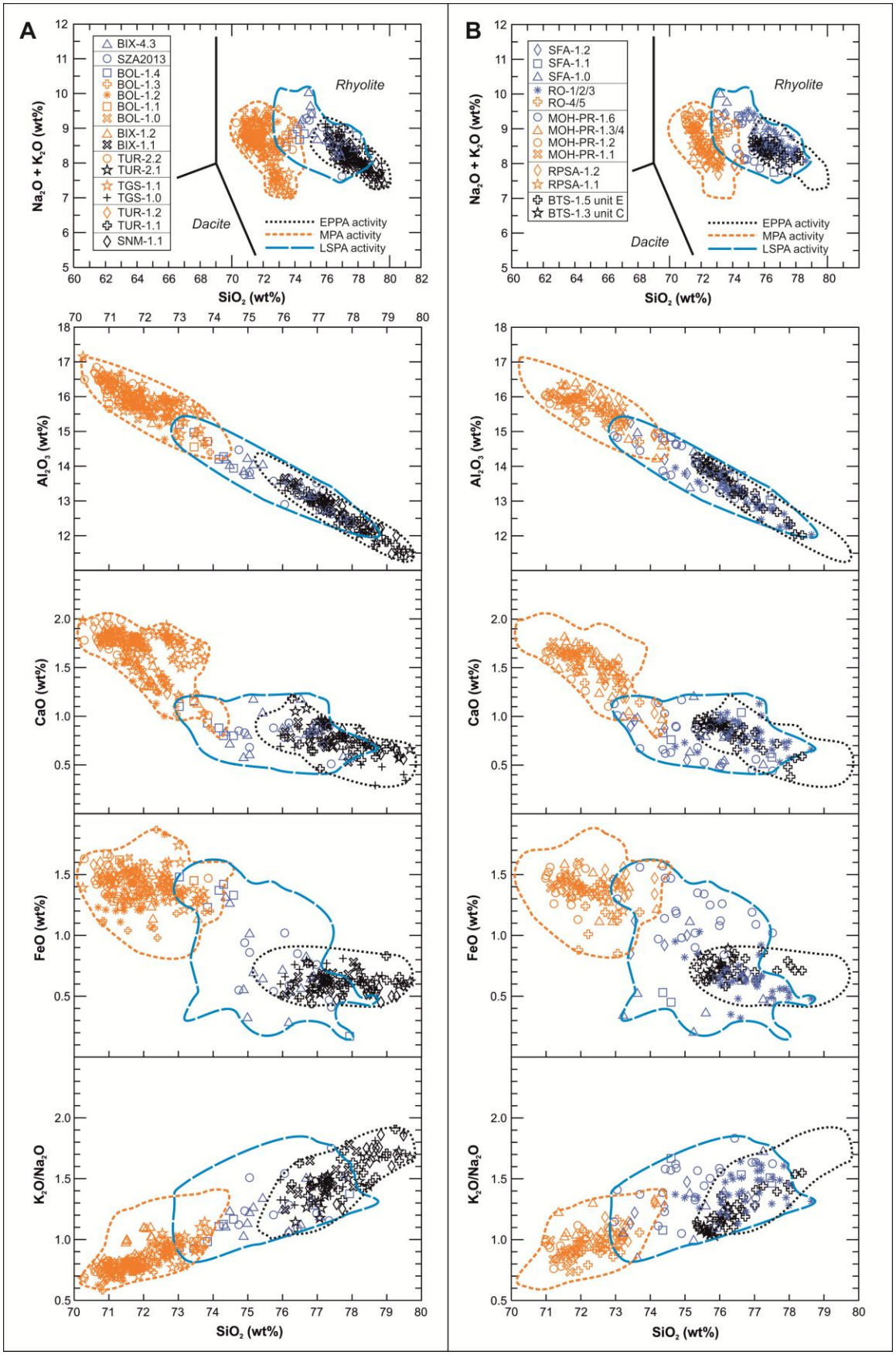

Figure 12

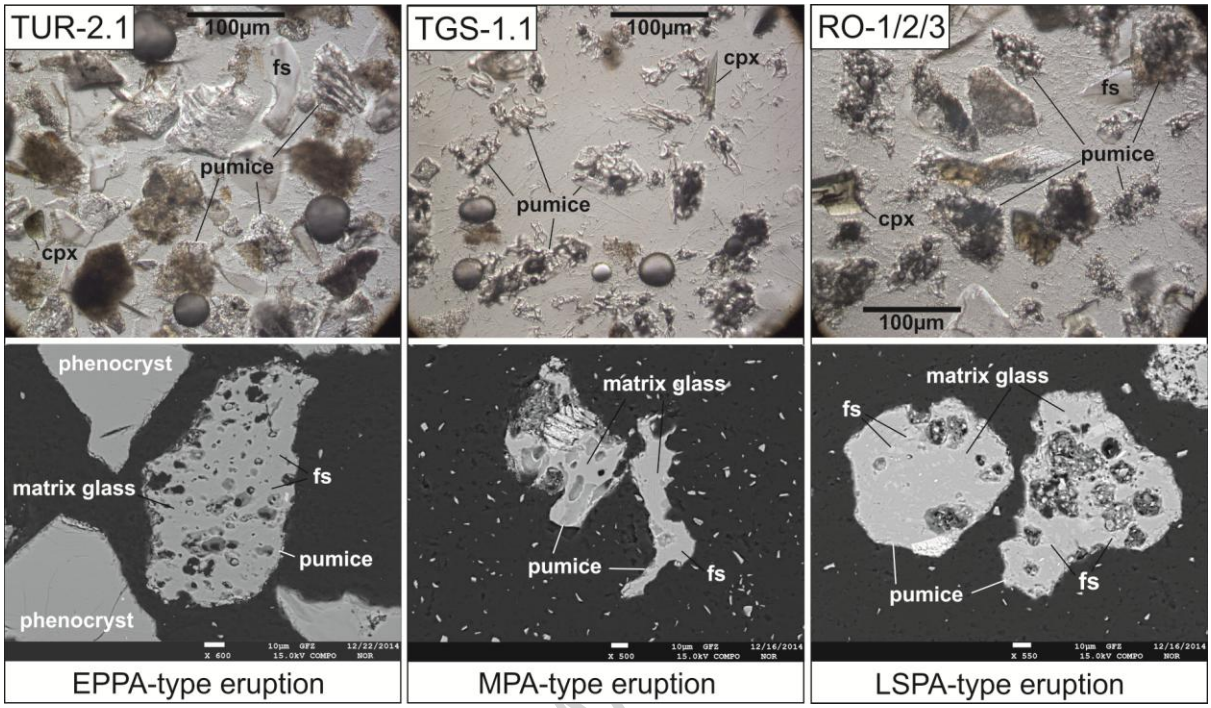

Figure 13

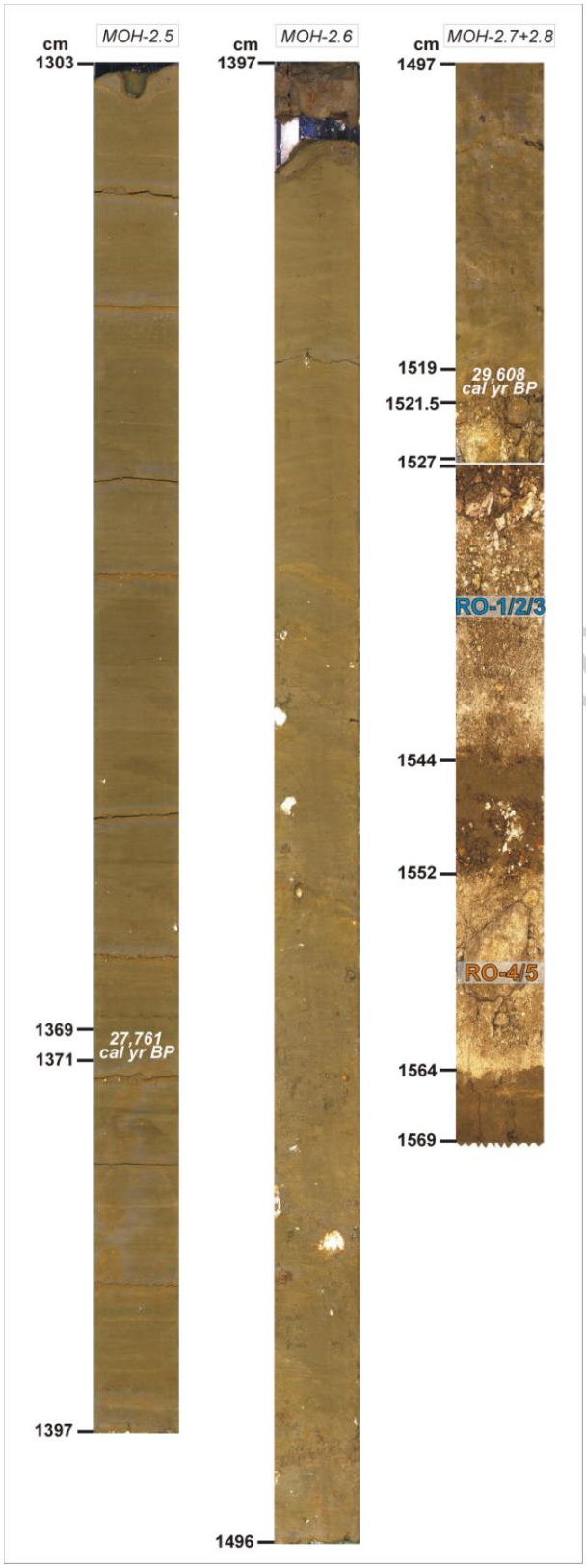

Figure 14

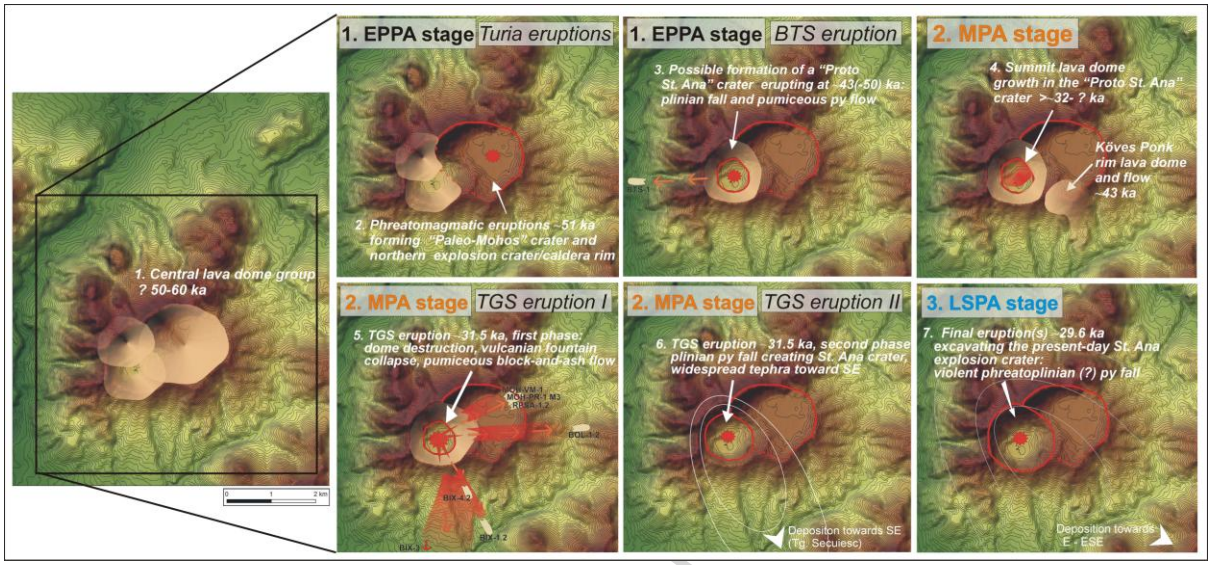

Figure 15

Table 1. Summary of volcanological and major element glass geochemical data of pyroclastic exposures around Ciomadul. For location, see text and Figs. 1 and 3. For description of units, see text. General references are given in the main text, only those specific to certain features appear here. Volcanic glass compositions, which are consistently rhyolitic, have been classified according to their main affinity (more silicic "EPPA"-, less silicic "MPA-" and intermediate silicic "LSPA-type", see text); n.a. = not analyzed; py = pyroclastic

Locality code; *lat. and long.*	**Pyroclastic unit in stratigraphic order (with thickness)**	**Grainsize characteristics**	**Type of rhyolitic volcanic glass**	**Interpretation (main depositional process)**
Proximal localities				
BTS-1 *46°07'55"N, 25°51'34.5"E*	1.7 'G' (~2 m)		n.a.	debris flow
	1.6 'F' (0.2–0.3 m)		n.a.	fluvial/hyperconcentrated flow
	1.5 'E' (~4 m) (subdivided into two by Szakács et al. 2015)	σφ=2.0, Mdφ= -0.8	EPPA	py flow (pumice flow)
	1.4 'D' (0.6–0.7 m)		n.a.	phreatoplinian py fall (Szakács et al. 2015)
	1.3 'C' (~4 m)	σφ=2.1, Mdφ= -1.3	EPPA	plinian pumice fall, slightly reworked on steep slope
	1.2 'B' (0.3 m)		n.a.	paleosol formed during humid period of Würm glacial
	1.1 'A' (0.5 m)		n.a.	fluvially reworked epiclastic deposit; terrace gravel acc. to Szakács et al. (1996)
BIX-1 *46°06'34.5"N, 25°54'38"E*	1.2 (3 to 5 m)	σφ=3.1, Mdφ= -2.0	MPA	pumiceous block-and-ash flow, valley infill
	1.1 (~6 m)		EPPA	fluvial reworking, intercalated by one or more phreatomagmatic(?) py fall, and overlain by debris flow
BIX-2 *46°05'59.5"N, 25°52'54.5"E*	(~3.5 m)		n.a.	block-and-ash flow
BIX-3 *46°05'21.5"N, 25°52'28"E*	(4 to 5 m)		n.a.	pumiceous block-and-ash flow
BIX-4 *46°06'58"N, 25°53'37"E*	4.3 (~0.5 m)		LSPA	vulcanian(?) py fall
	4.2 (~2.5-3 m)		n.a.	pumiceous block-and-ash flow
	4.1 (~8 m)		n.a.	subsequent phreatomagmatic (e.g. vulcanian?) py falls
BOL-1 *46°07'46"N, 25°55'53"E*	1.4 (~0.2 m)		LSPA	vulcanian(?) py fall
	1.3 (~0.15 m)		MPA	slightly reworked py fall
	1.2 (~0.3 to 0.4 m)	σφ=1.9, Mdφ= -3.0	MPA	pumiceous block-and-ash flow
	1.1 (0.5 to 1 m)		MPA	subsequent and partly coeval py falls and py surges
	1.0 (~4 m)		MPA	pumiceous py flow and py surges
MOH-PR-1 *46°08'11"N, 25°54'34.5"E*	1.9 M7C (~0.3 m)		n.a.	reworked?) pumice fall
	1.8 M7A, B (~0.4 m)		n.a.	lacustrine sedimentation, tephra reworking
	1.7 M6B (~0.7 m)		n.a.	lacustrine sedimentation, tephra reworking
	1.6 M6A (~0.5 m)		LSPA	pyroclastic fall
	1.5 M5 (~0.5 m)		MPA	lacustrine sedimentation, tephra reworking
	(not sampled) M4 (~0.4 m)		MPA	lacustrine sedimentation, tephra reworking
	1.3/1.4 M3 (3.5 to 4 m)	σφ=2.6, Mdφ= -2.4	MPA	pumiceous block-and-ash flow
	1.2 M2 (~2.5 m)		MPA	pumiceous block-and-ash flow
	1.1 M1 (~2 m)		MPA	subsequent (or partly coeval) py falls and py surges
	1.0 M0 (~0.9 m)		n.a.	pumice fall, possibly phretomagmatic
MOH-VM-1 *46°08'13.5"N, 25°54'34.5"E*	1.3 (~1.5 m)	upper: σφ=2.5, Mdφ= -3.0 lower: σφ=2.2, Mdφ= -1.0	n.a.	pumiceous block-and-ash flow
	1.2 (~2 m)		n.a.	pumiceous block-and-ash flow
	1.1 (~0.5 m)		n.a.	subsequent (or partly coeval) py falls and py surges
RPSA-1 *46°08'05''N, 25°54'41"E*	1.2 (~3 m)	upper: σφ=2.9, Mdφ= -2.4	MPA	pumiceous block-and-ash flow

		lower: σφ=2.7, Mdφ= -2.1		
	1.1 (~1.5 m)		MPA	subsequent (or partly coeval) py falls and py surges
SFA-1 *46°07'52"N, 25°53'37.5"E*	1.3 (lithoclasts)		n.a.	(lithic clasts from 1.2)
	1.2 (~0.3 m)		LSPA	slightly reworked phreatomagmatic py fall
	1.1 (~0.2 m)		LSPA	py fall
	1.0 (~0.2 m)		LSPA	phreatomagmatic py fall
Medial/distal localities				
TGS-1 *46°00'55"N, 26°07'44"E*	1.1 (0.3 to 0.4 m)	upper: σφ=1.9, Mdφ= -1.5 lower: σφ=1.4, Mdφ= -1.1	MPA	plinian pumice fall
	1.0 (~2-3 m)		EPPA	phreatomagmatic py falls, slight reworking
TUR-1 *46°01'05.5"N, 26°05'23"E*	1.2 (<10 cm)	σφ=2.4, Mdφ= -1.8	MPA	pumice fall
	1.1 (8 m)		EPPA	laharic and normal fluvial reworking of py fall sequence
TUR-2 *46°03'18.5"N, 26°01'17"E*	2.3 (~5 cm)		n.a.	slightly reworked py fall
	2.2 (<10 cm)	σφ=2.2, Mdφ= -1.5	MPA	pumice fall
	2.1 (~1.5 m)	σφ=1.2, Mdφ=0.9	EPPA	py fall and py surge sequence, minor fluvial reworking
SNM-1 *46°16'43"N, 25°55'00"E*	1.2 (~0.5 m)	σφ=1.7, Mdφ=2.2	n.a.	phreatomagmatic py fall
	1.1 (~15 cm)	σφ=0.7, Mdφ=0.3	EPPA	phreatomagmatic py fall

Table 2:

Comparison of (U-Th)/He, ^{14}C and luminescence age constraints of the past ~50 ky volcanic rocks of Ciomadul volcano

Unit/layer name	Unit type	Dated material / fraction		Radiometric age						Proposed eruption age (ka)
				^{14}C			*Zircon (U-Th)He dating*		*OSL*	
				^{14}C yr BP	Calibrated 2σ age range cal yr BP (IntCal13)[7]	Mean calibrated age in cal yr BP with 2σ range [x]	Disequilibrium age (ka) range of individual grains[6] (in brackets: number of grains)	Disequilibrium age[6] (ka)	OSL age (ka)	
BOL- 1.1		zircon crystals from pumice					48.5 – 69.5 (5)	55.9 (+2.2, -2.3)		**? (~32)**
TUR-2.1	py fall	overlying loess							4-11 µm: 36.3±3.3 [x]	**≤ 51**
		underlying loess							4-11 µm: 51.0±4.8 [x]	
BTS-1.5 unit 'E'	py flow	charcoal		>35,770[1,*]	>40,024–40,796	>40,410±386				**~43**
		charcoal		>35,520[1,*]	>39,746–40,484	>40,115±369				
		charcoal		38,700±1000[4]	41,241–44,413	42,827±1586				
BTS-1.3 unit 'C'	py fall	zircon crystals from pumice					43.4 – 63.9 (8)	50.3 (+1.3,-1.2)		**? (~43)**
		underlying paleosoil		>36,770[2*]	>41,115–41,700	>41,408±292				
		underlying paleosoil		>42,650[2*]	>45,471–46,256	>45,864±392				
Piscul Pietros (Köves Ponk)	lava flow	zircon crystal from massive rock					37.2 – 49.3 (4)	42.9 (+1.4,-1.5)		**~43**
BIX 1.2	py flow	charcoal		27,040±450[3]	30,216–31,879	31,048±831				**~31.5**
		charcoal		27,200±260[4]	30,833–31,482	31,158±324				
		humic acid		28,050±290[4]	31,277–32,744	32,011±733				
		charcoal		27,550±270[4]	30,979–31,936	31,458±478				
		humic acid		27,910±280[4]	31,190–32,567	31,879±688				
		zircon crystals from pumice					28.0 – 41.9 (5)	32.6 (+1.0,-1.0)	32.61 (±1.05)**	
MOH-PR-1.3 (M3)	py flow	zircon crystals from pumice					29.7 – 42.3 (8)	34.0 (+1.0,-0.9)	32.65 (±1.02)**	**~31.5**
		(M5c) overlying clayey sand							4-11 µm: 33.9±2.2 [x]	
		(M35) overlying clayey sand							4-11 µm: 19.6±1.3 [x]	
TGS 1.1	py fall	zircon crystals from pumice					36.6, 37.0, 43.7, 75.8, 118, 137.4	38.9 (+1.6,-1.8) (based on the 3 youngest grains)		**? (~31.5)**
		over-lying loess	5 cm above						4-11 µm: 24.1±2.3 [x]	
			ca. 30 cm above						4-11 µm: 35.9±2.9[6]	

		under-lying loess	5 cm below						4-11 μm: 30.7±3.0 [X]	
			ca. 35 cm below						4-11 μm: 43.3±3.0 [6]	
MOHOS CORE:	***lab code***									
MOH-2.5	COL3252.1.1	charcoal fragment 1369-1371 cm		23,529±348 [X]	27,136 – 28,387	27,762±625				
MOH-2.7	COL3253.1.1	bulk sediment 1519-1521.5 cm		25,438±207 [X]	28,987 – 30,206	29,597±610				
RO-1/2/3	tephra layer									**~29.6**
RO-4/5	tephra layer									**(~31.5)**
ST. ANA CORE:	***lab code***									
SZA-2010	COL1128.1.1	organic remains 1662 cm***		21,685±163 [5]	25,643 – 26,249	25,946±303				
SZA-2013-08/1	DeA-4967	pollen extract 1816-1817 cm****		20,493±167 [X]	24,218 – 25,189	24,704±485				
SZA-2013-08/2	DeA-5403	pollen extract 1829-1830 cm****		18,411±126 [X]	21,926 – 22,510	22,218±292				
SZA-2013-09/1	DeA-5408	pollen extract 1977-1979 cm****		17,845±178 [X]	21,054 – 22,077	21,566±511				
SZA-2013-09/2	DeA-4968.1.2	pollen extract 2031.5-2034.5 cm****		22,949±217 [X]	26,719 – 27,642	27,180±462				
SZA-2013-10/1	DeA-5074	pollen extract 2140-2145 cm****		18,447±136 [X]	21,927 – 22,567	22,247±320				

[1] Moriya et al. (1995), [2] Moriya et al. (1996), [3] Vinkler et al. (2007), [4] Harangi et al. (2010), [5] Karátson et al. (2013), [6] Harangi et al. (2015), [7] according to Reimer et al. (2013)
[X] this study; for radiocarbon dating, calibration was made according to Stuiver and Reimer (2013)

* in case of missing error estimates, ±100 years measurement error was used in the calibration
** weighted mean age using the mean square weighted deviation method ($1/\sigma^2$; this study), if considering the given individual errors in Harangi et al. (2015) as 1σ
*** adjusted depth including 6 m water column (see Magyari et al., 2014 for details)
**** raw depths recorded at coring including 6 m water column

Highlights of the manuscript *The latest explosive eruptions of Ciomadul (Csomád) volcano, East Carpathians - a tephrostratigraphic approach for the 51–29 ka BP time interval*

→ Field volcanology, EPMA, OSL and 14C data constrain the latest <51 ka explosive eruptions

→ A ~31.5 ka BP two-phase eruption was followed by a newly discovered ~29.6 ka BP eruption

→ Coring and dating of Ciomadul's twin craters can be used for tephrostratigraphy